Atomization and Sprays, 24 (4): 303–348 (2014)

INJECTION OF WATER-IN-OIL EMULSION JETS INTO A SUBSONIC CROSSFLOW: AN EXPERIMENTAL STUDY

Chris D. Bolszo, Vincent G. McDonell,* Guillermo A. Gomez, & G. Scott Samuelsen

Department of Mechanical and Aerospace Engineering, University of California, Irvine, California 92697-3550, USA

*Address all correspondence to Vincent G. McDonell
E-mail: mcdonell@ucicl.uci.edu

Original Manuscript Submitted: 8/6/2013; Final Draft Received: 11/13/2013

In this work, the influence of introducing water in oil, as an emulsion, in a liquid jet injected into a gaseous crossflow is investigated. Of particular interest is the relationship between emulsion characteristics on spray penetration and spray droplet size. Tests are conducted at atmospheric conditions, with liquid jet-to-crossflow momentum flux ratios spanning 30–120, and water addition to 40% by mass. Gas velocities range from 20 to 80 m/s and liquid velocities from 10–20 m/s are considered. Backlit high-speed video is used to document the overall spray characteristics and laser diffraction is used to measure the spray droplet sizes. Sobel edge filtering and intensity thresholding are utilized to establish the spray plume upper edge for the spray morphology, which was used to establish the spray trajectory. The Buckingham π theorem is used to identify the important functional groupings for the current physical problem. For time-averaged trajectories, an existing liquid jet trajectory equation form from Wu and co-workers successfully correlates the penetration of emulsion spray plumes. These findings show that momentum flux of the bulk emulsion jet remains the dominant factor governing jet penetration. The influence of emulsification on spray plume droplet size distributions is quantified in the current work. A new nondimensional quantity is proposed to account for the effect of body forces and repulsive interfacial tension on correlating breakup. For the conditions studied, an additional primary breakup mode for emulsions, interfacial tension breakup, is identified and observed to influence spray plume development and droplet size.

KEY WORDS: *jet in crossflow, jet penetration, droplet size, interfacial tension, laser diffraction spectroscopy, high-speed cinematography, Buckingham π theorem*

1. INTRODUCTION

In many applications, liquid atomization is achieved by injecting a column of liquid as a plain jet, perpendicularly (or angles near to) into a gaseous flow. This strategy has been utilized for various combustion systems including rocket propulsion, turbofan, turbojet,

NOMENCLATURE

A	area
d	nozzle diameter
F	force
g	gravity force
h	channel height
K	viscosity ratio
[L]	length
$\dot{m}$	massflow
[M]	mass
P	pressure
q	momentum flux ratio
S	emulsion tension-to-body force parameter
t	time
T	temperature
$[T]$	time
U	mean velocity
V	volume
x	downstream distance
y	vertical distance
Z	emulsion interfacial-to -surface tension parameter

Greek Symbols

$\dot{\gamma}$	shear rate
μ	viscosity
$[\mu]$	intrinsic viscosity
Π	nondimensional grouping
ρ	density
σ_i	interfacial tension
σ_s	surface tension
ϕ	volume fraction
ϕ_m	maximum packing efficiency
Φ	water mass fraction

Dimensionless numbers and abbreviations

Bo	Bond number
C_d	discharge coefficient
C_D	drag coefficient
Ca	capillary number
D_{32}	Sauter mean diameter
D_{32d}	discrete phase Sauter mean diameter
DF2	low sulfur diesel distillate #2
kT	thermal energy
Mu	multiphase Bond number ($\mathrm{Bo}_e/\mathrm{Bo}_{l-g}$)
Pe	Peclet number
Re	Reynolds number
Oh	Ohnesorge number
We	Weber number

Subscripts

aero	aerodynamic
c	continuous
d	discrete
D	drag
e	emulsion
g	gas
i	interfacial
l	liquid
o	discharge
P	particle
r	relative
s	surface
w	water

ramjet, scramjet engines/afterburners, and power generation by industrial gas turbines. Therefore, it is of interest to understand the breakup, atomization, and trajectory of the liquid fuel in order to improve control over the subsequent heat release. The jet in a crossflow problem has been studied for half a century (Leong, 2000; Leong et al., 2001). Progress on understanding this injection strategy involves investigating and modeling the liquid breakup and resulting spray plume structure. Studies that have elucidated the governing physics provide a means for predicting the overall spray shape utilizing physical–empirical correlations (Adelberg, 1967; Schetz and Padhye, 1977). One of the earliest spray trajectory correlations was presented by Geery and Margetts (1969). Correlation equations have proposed different forms of influencing variables, grouping of variables to predict liquid trajectories within the gaseous environment (Wu et al., 1998; Becker and Hassa, 2002).

As liquid is introduced perpendicularly into a low Weber number gaseous crossflow, interaction of the fluid streams occurs. Figure 1 presents a schematic of the breakup of a liquid jet in crossflow at low aerodynamic Weber numbers (We_{aero}), adapted from Wu

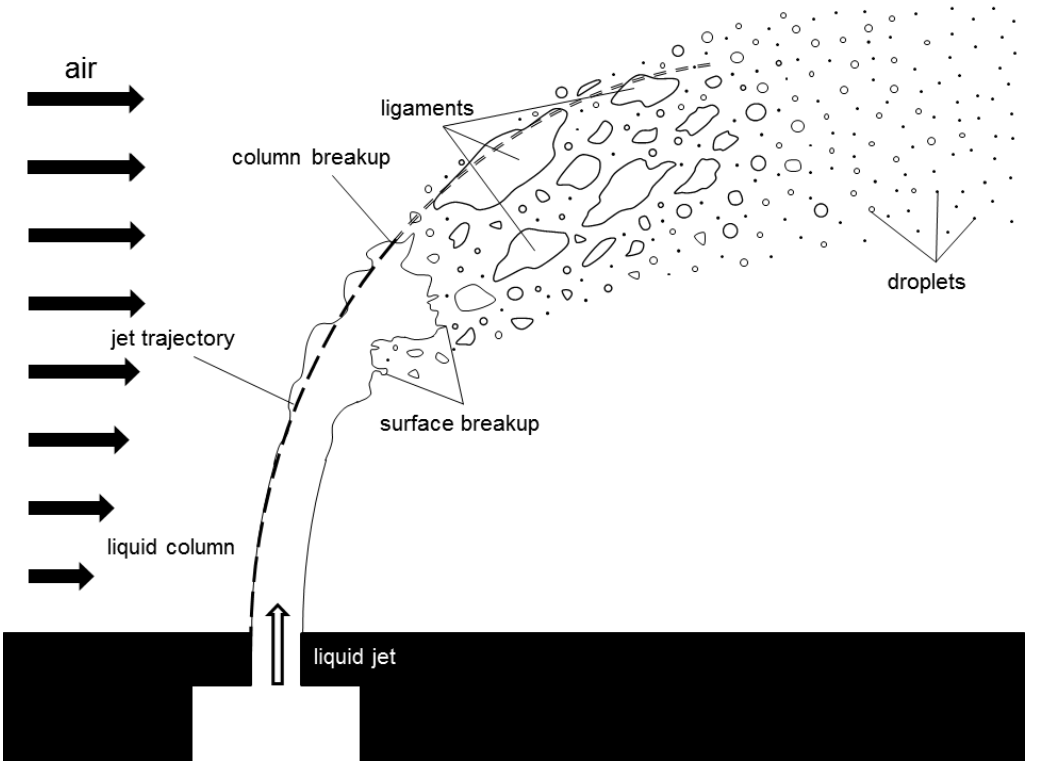

FIG. 1: Representative schematic of primary breakup in a liquid jet-in-crossflow at low We_{aero} values, adapted from Wu et al. (1998).

et al. (1997) as representative of the primary breakup processes. Secondary bag-type breakup is not included in the present diagram.

At these conditions (Fig. 1), as the liquid column exits from the initial point of injection along the wall it begins to deform, growing unstable, breaking up and dispersing within the crossflow stream. The momentum interaction of both fluids break up the jet as the gas flow carries liquid downstream The upper liquid trajectory boundary line is provided as a time-averaged representation of the liquid penetration into the crossflow. Considering the primary jet breakup modes, the column breakup mode is predominantly responsible for breakup as the liquid encounters the gas stream at low We_{aero} values. The liquid jet bends with the crossflow streamlines and, along its surface, a Kevin–Helmholtz instability develops (Wu et al., 1998; Herrmann, 2010). As the instability grows, the column thins and eventually pinches off parcels of fluid, forming ligaments, which then elongate and pinch apart into droplets. The pinch-off location is signified by the change in dotted line type along the averaged upper trajectory outline in Fig. 1.

As We_{aero} values increase sufficiently higher, liquid is stripped off of the column surface due to the increased contribution to air shearing forces, as shown in Fig. 2. The liquid undergoes a transfer of momentum from the crossflow, resulting in a downstream liquid trajectory as it penetrates into the gaseous flow, creating a shallower penetration

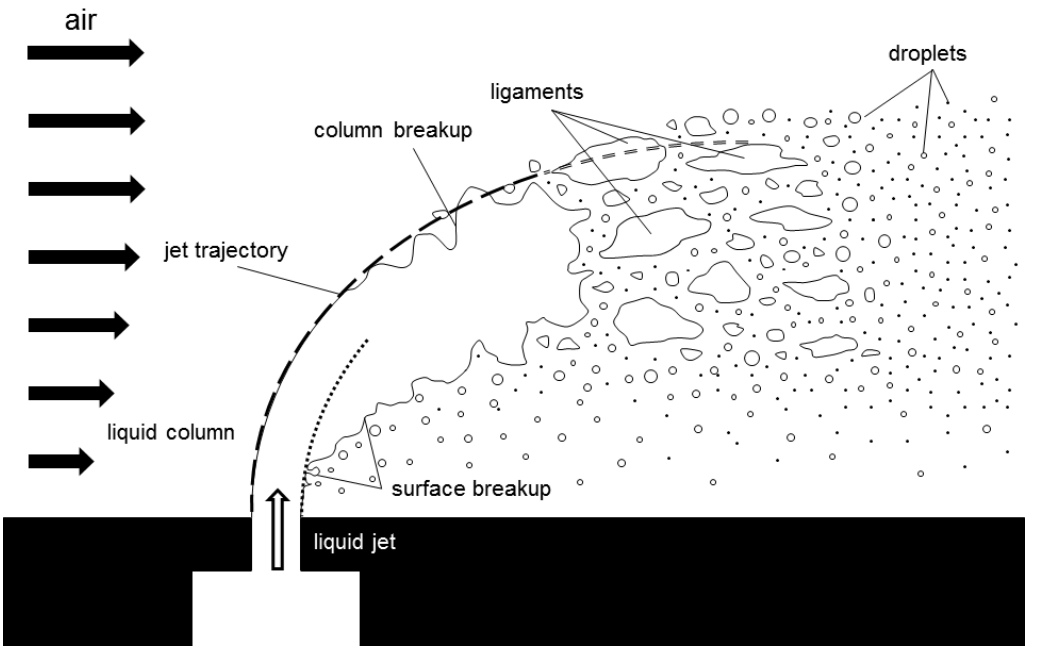

FIG. 2: Representative schematic of primary breakup in a liquid jet-in-crossflow at high We_{aero} values.

and a trajectory with greater curvature. Surface breakup mode occurs as gas momentum interacts at the liquid surface, flattening the column shape (note the dashed lines tracing the windward and leeward edges of the column centerline) from a circle into an ellipse and stripping droplets off of the column in Fig. 2 (Clark, 1964). Droplets are also sheared off the column as the liquid deforms along its trajectory, which undergo further deformation and secondary atomization via mainly the bag-type breakup mechanisms (Jalaal and Mehravaran, 2012) to produce the final droplet size within the plume (Hinze, 1955; Krzeczkowski, 1980).

By comparing the inertia of the fluids involved, the liquid breakup behavior can be characterized by considering the momentum flux ratio (q), Eq. (1). This dimensionless quantity is the ratio of the liquid to the gaseous crossflow momentum flux, where ρ and U are density and mean velocity of the liquid and gaseous streams, respectively.

$$q = \frac{\rho_l U_l^2}{\rho_g U_g^2} \tag{1}$$

The aerodynamic Weber number ($\mathrm{We}_{\mathrm{aero}}$), defined in Eq. (2), classifies jet breakup due to air shearing by the crossflow, becoming more significant as gas density increases (Lubarsky et al., 2010) and surface tension decreases (Stenzler et al., 2003). $\mathrm{We}_{\mathrm{aero}}$ considers incompressible air density (ρ_g), mean crossflow velocity (U_g), nozzle diameter (d), and liquid surface tension (σ).

$$\mathrm{We}_{\mathrm{aero}} = \frac{\rho_g U_g^2 d}{\sigma_s} \tag{2}$$

The regimes of breakup due to column and surface breakup modes have been correlated with q and $\mathrm{We}_{\mathrm{aero}}$ as proposed by Wu et al. (1998) in Fig. 3. Depending on the values of these parameters, surface breakup mode, column breakup mode, or both primary modes can be important in the spray plume development downstream of the jet orifice.

Modeling approaches of jet column breakup, penetration, and atomization in a crossflow have evolved as a result of experimental studies and analyses to understand and predict resultant liquid dispersion. In particular, the evolution of high-speed visualization methods have led to improved understanding of the breakup of jets-in-crossflow, by capturing breakup phenomena at their corresponding fast (μs) time scales (Brown and McDonell, 2006). The visualization of the breakup process has allowed for "validation" of advanced numerical simulations of the primary breakup modes (Herrmann, 2010).

The Ohnesorge number (Oh) and Reynolds number (Re) are also used to capture the role of friction versus surface and inertial forces during interaction of the gas and liquid. Equations (3) and (4) define these dimensionless groups for a given set of fluids. In the practical application of jet in crossflow in combustion devices, a high momentum

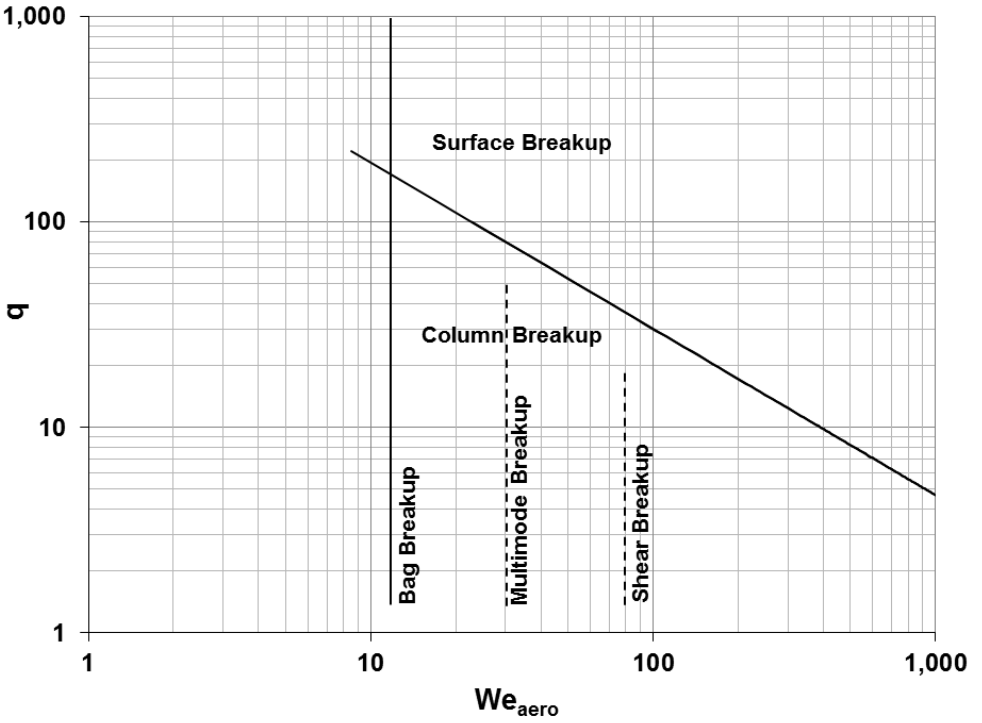

FIG. 3: q vs. $\mathrm{We}_{\mathrm{aero}}$ regime plot (Wu et al., 1998).

air stream is used to break up a liquid column even at low liquid injection pressures. A large momentum contribution toward breakup can occur from either the liquid or the gaseous fluid, which results in the liquid [or nozzle Reynolds number (Re_l)] and gaseous Reynolds number (Re_g), or both, being important. The liquid will produce a greater friction force at these flow rates, and thus Oh_l is often considered for gas turbine applications.

$$\mathrm{Re} = \frac{\rho U d}{\mu}, \tag{3}$$

$$\mathrm{Oh}_l = \frac{\mu_l}{\sqrt{\rho_l \sigma_s d}}. \tag{4}$$

In the development of understanding the liquid jet in crossflow, pure (i.e., homogeneous) liquids have generally been studied. In the present work, the behavior of oil–water emulsions is of interest. As a result, the objective of the present work is to determine the fluid properties which govern the breakup of $emulsions$ and ascertain the degree to which they can correlate with measured penetration and droplet size data. Results are compared with existing correlations that have been developed for homogeneous liquids

and deviations in trends are utilized quantitatively to corroborate the additional physical breakup processes for emulsions. To assess this, high-speed imaging and laser diffraction are used to quantitatively and qualitatively evaluate the behavior of emulsion liquid jets with varying characteristics. The high-speed images are analyzed for penetration tendencies of emulsions which are compared to those predicted by previously developed correlations for homogeneous liquids. The laser diffraction measurements are used to develop a physics-based empirical correlation to predict the droplet size within the spray plume and the influence of emulsion characteristics on droplet size.

2. CORRELATION FRAMEWORK

As a first step in the consideration of the behavior of emulsions, the extent to which correlations derived for homogeneous liquids can describe basic spray plume parameters such as penetration are assessed. Many forms of penetration equations have been developed by different groups under different experimental conditions. One of the earliest correlations by Geery and Margetts, presented in a generalized form Eq. (5), equates a simple dimensionless relation that includes the momentum flux ratio, nozzle diameter, and downstream distance (x) to predict the penetration height (y). The correlation presented by Wu and co-workers (1998) arrived at the same form [Eq. (5)] from their extensive experimental study of liquid jets in air crossflows at low Mach numbers (Wu et al., 1998). The data used to develop this correlation featured values of q from 5 to 50. Becker and Hassa (2002) and co-workers (Rachner et al., 2002) provided a slightly modified version using data at elevated pressure with q varying from 1 to 40, provided as Eq. (6). Additional correlations by Stenzler et al. (2003) and Birouk et al. (2007) included the effect of $\mathrm{We}_{\mathrm{aero}}$ and viscosity on trajectory predictions; these forms are represented in Eqs. (7) and (8). Work by Lee et al. (2007) investigated the penetration of round turbulent jets in a crossflow over a large range of q from 3 to 200 and included the liquid column drag coefficient (C_D) as shown in Eq. (9), which was set to a constant value of 3 for shear breakup.

$$\frac{y}{d} = aq^b \left(\frac{x}{d}\right)^c, \tag{5}$$

$$\frac{y}{d} = aq^b \ln\left[1 + c\left(\frac{x}{d}\right)\right], \tag{6}$$

$$\frac{y}{d} = aq^b \left(\frac{x}{d}\right)^c \mathrm{We}_{\mathrm{aero}}^e \left(\frac{\mu_l}{\mu_w}\right)^f, \tag{7}$$

$$\frac{y}{d} = aq^b \left(\frac{x}{d}\right)^c \left(\frac{\mu_l}{\mu_w}\right)^e, \tag{8}$$

$$\left(\frac{y}{dq}\right) = \sqrt{\frac{\pi}{C_D}} \left(\frac{x}{dq}\right)^a. \tag{9}$$

The observation of the various forms of expressions that have been found to correlate penetration of homogeneous liquids leads to the question of what is giving rise to a lack of consensus on the role of the various terms. As a result, a more generalized consideration of the phenomena contributing to the liquid jet behavior is worth evaluating. This can also serve as a broader starting point in consideration of the role of the emulsion in the process.

Distinguishing between emulsion and pure liquid properties, the emulsion density (ρ_e) is defined by considering the volume (V) from the liquid densities of both the discrete and continuous components, as shown in Eq. (10). Emulsification introduces an interfacial tension (σ_i) as discrete droplets populate the liquid, creating an internal flow resistance due to the presence of the liquid–liquid boundaries. Due to the presence of the internal droplet distribution within the continuous component liquid, the emulsion viscosity is a function of the rate of shear, which introduces a departure from Newtonian fluid behavior. The work of Ouchiyama and Tanaka (1980–1984) and Pal (1997) provides a theoretical development for the calculation of a relative viscosity based on the fluid properties, namely, volume concentration, discrete droplet size distribution, and sphere packing efficiency (ϕ_m) (Ouchiyama and Tanaka, 1980; Pal, 1998) as shown in Eq. (11). The proportional terms to equate a relative viscosity are as follows: the shear rate ($\dot{\gamma}$), the time evolution of shear (t), the respective discrete (μ_d) and continuous component viscosity (μ_c), the discrete representative droplet diameter, shown here as the Sauter mean diameter (D_{32d}), the discrete volume fraction (ϕ), and the thermal energy (kT).

$$\rho_e = \frac{V_d\rho_d + V_c\rho_c}{(V_d + V_c)} = \rho_l, \tag{10}$$

$$\mu_l \sim f(t, \dot{\gamma}, \mu_c, \mu_d, \rho_c, \rho_d, D_{d32}, \phi, kT, \sigma_i). \tag{11}$$

Next, consider the physical dependency of fluid properties for the jet in crossflow flow configuration. For emulsions consisting of light oils and water, like those used in the current study, the departure from non-Newtonian is minimal in terms of its stress–strain relationship and therefore may be treated as simply deviations in the Newtonian fluid framework. This conclusion is proven here for a water-in-oil emulsion through a dimensional consideration of the forces governing viscosity for a practical water-in-fuel oil emulsion via the nondimensionalization of Eq. (11), which uses the same approach as Krynke and Sek (2004). The emulsion particle Peclet number (Pe_P), particle capillary number (Ca_P), and particle Reynolds number (Re_P) are defined in Eqs. (12) and (13). Considering macroemulsions, with discrete droplets greater than 1 μm in diameter, the effect of Brownian motion on droplets will be small, and therefore Pe_P can be neglected.

$$\frac{\mu_l}{\mu_c} \sim f\left[\frac{t}{\mu_c\left(D_{32d}\right)^3/8KT}, K, \rho_r, \frac{\mu_c\dot{\gamma}\left(D_{32d}\right)^3}{8kT}, \frac{\rho_c\dot{\gamma}D_{32d}}{2\mu_c}, \frac{\mu_c\dot{\gamma}D_{32}d}{2\sigma_i}, \phi\right], \tag{12}$$

$$\frac{\mu_l}{\mu_c} \sim f(t_r, K, \rho_r, \mathrm{Pe}_P, \mathrm{Re}_P, \mathrm{Ca}_P, \phi), \tag{13}$$

The value of Ca_P tends toward zero for low viscosity water in low and medium distillate fuel oil emulsions with a viscosity ratio ($K = \mu_d/\mu_c$) near unity, allowing a Ca_P dependence to also be removed when not considering very high shear rates during flow. The densities of oil and water are similar, which typically approach unity ($\rho_r = \rho_d/\rho_c$). The reduced time tends toward infinity during steady-state flow conditions, resulting in a minute contribution from dissipation forces. The consideration of these arguments allows a straightforward method to determine the emulsion viscosity with three dimensionless groupings [Eq. (14)].

$$\mu_r \sim f(K, \mathrm{Re}_P, \phi). \tag{14}$$

The emulsion viscosity has been normalized as a relative viscosity by the continuous medium ($\mu_r = \mu_l/\mu_c$) according to the Krieger–Dougherty equation form (Krieger and Dougherty, 1959), presented in Eq. (15), where the maximum intrinsic viscosity ($[\mu]$) has a value of 2.5. However, determining the emulsion viscosity in dynamic flowing systems like a jet in crossflow presents a significant challenge due to the inability to probe the flow nonintrusively. Macroemulsions are opaque, which obstructs the determination of the internal discrete droplet size distribution. Fluid samples and magnified measurements of stabilized emulsion discrete droplet sizes are usually preformed to establish the emulsion composition.

$$\mu_r = \left[1 - \frac{\phi}{\phi_m}\right]^{-[\mu]\phi_m}. \tag{15}$$

In Eq. (16), the bulk emulsion liquid velocity (U_l) is a function of the discharge pressure drop of the nozzle (ΔP_l); the resultant mass flow of both liquid components are equated in terms of the liquid discharge coefficient (C_{dl}), the liquid density from Eq. (10), viscosity determined through Eq. (15), and the gravitational body force (g).

$$U_l \sim f(d, \Delta P_l, \rho_l, \mu_l, \sigma_i, \phi, C_{dl,} g). \tag{16}$$

In Eq. (17), the gaseous mean velocity (U_g) can be represented by considering the cross-sectional area, or channel height (h) in two dimensions, the pressure drop across the crossflow test section (ΔP_g), the gaseous density (ρ_g), viscosity (μ_g), and the cross-section discharge coefficient up the entrance into the test section (C_{dg}). The actual velocity distribution of a wide crossflow channel will approach U_g with increasing h and will also decrease the influence of the far wall on the flow.

$$U_g \sim f(h, \Delta P_g, \rho_g, \mu_g, C_{dg}), \tag{17}$$

2.1 Application to Penetration of an Emulsion Jet in Crossflow

The governing relationships for evaluation of the flow properties associated with the jet in crossflow test section have been formalized dimensionally. Identifying the physics responsible, it is now possible to introduce the gaseous and emulsions streams and dimensionally formulate their interaction. In order to understand the governing physics of the penetration (y) of an emulsion jet in crossflow, Eq. (18) introduces the flow properties of primary interest. As shown, in addition to the liquid and gaseous properties, the force of drag (F_D) and the body force due to gravity (g) on the liquid, as well as the interfacial tension (σ_i) due to introducing a large volume of dispersed droplets as an emulsion, are presented. It is assumed that $h \gg d$, thus the far wall does not influence the spray trajectory. Hence, this dependence can be removed, allowing the penetration height of the trajectory y to be directly compared with d as a length scale.

$$y \sim f(d, x, \rho_l, \rho_d, \rho_g, U_l, U_g, \mu_l, \mu_g, \sigma_s, \sigma_i, D_{32d}, \Phi, F_D, g). \tag{18}$$

Using the Buckingham π theorem (Appendix) to evaluate the dimensional relationship of the proposed terms in Eq. (18), 13 dimensionless groupings result due to the involvement of three reference dimensions ([L], [M], and [T]) with 16 fluid variables. These nondimensional groupings are shown in Eq. (19), which are all independent quantities that compare the governing processes involved in the emulsion jet in crossflow problem and comprise normalized length scales. In determining the liquid penetration into the air flow stream as quantified by the spray trajectory (y/d), the significant terms are the normalized lengths in x and y, the momentum flux ratio, the aerodynamic Weber number, the liquid Ohnesorge number, the Reynolds number of the liquid, the Reynolds number of the gas phase, the liquid-to-gas Bond number (Bo_{l-g}), the emulsion bond number (Bo_e), and the drag coefficient (C_D).

For an emulsion, the additional repulsive force due to the hydrophobicity of the continuous oil component counteracts the liquid cohesion forces due to the surface tension. This is represented by the interfacial-to-surface tension ratio (σ_s/σ_i). Overall, the surface-to-interfacial force balance is dependent on the amount of the discrete phase in proportion to the continuous phase, represented by the total mass fraction of the discrete component (Φ). The length scale of interest for the interaction of the interfacial forces is the discrete droplet diameter, which is normalized by the initial jet diameter (D_{32d}/d). These terms, which represent the direct influence of the emulsion's effect on the spray, are grouped as a single term $Z = f(\sigma_s/\sigma_i,\ D_{d32}/d, \Phi)$. The difference in density between the components as dispersion produces a separation in local concentration, which has been studied at length for the injection emulsion sprays (Bolszo, 2011) and is represented by the discrete-to-continuous component density difference in the emulsion Bond number (Bo_e). Further, the role of the surface-to-body forces between the liquid and gas is represented by a liquid-to-gas Bond number (Bo_{l-g}). The dependence on penetration for emulsions is provided in Eq. (20).

$$\frac{y}{d} \sim f\left(\frac{x}{d}, \frac{\rho_l U_l^2}{\rho_g U_g^2}, \frac{\rho_g U_g^2 d}{\sigma_s}, \frac{\mu_l}{\sqrt{\rho_l \sigma_s d}}, \frac{\rho_g U_g d}{\mu_g}, \frac{\rho_l U_l d}{\mu_l}, \frac{D_{d32}}{d}, \Phi, \frac{\sigma_s}{\sigma_i}, \frac{(\rho_l - \rho_g) g d^2}{\sigma_s}, \frac{(\rho_d - \rho_c) g D_{32d}^2}{\sigma_i}, \frac{F_D}{\rho_g U_g^2 d^2}\right), \tag{19}$$

$$\frac{y}{d} \sim f\left(\frac{x}{d}, q, \mathrm{We}_{\mathrm{aero}}, \mathrm{Oh}_l, \mathrm{Re}_g, \mathrm{Re}_N, Z, \mathrm{Bo}_{l-g}, \mathrm{Bo}_e, C_D\right). \tag{20}$$

2.2 Application to Droplet Size of an Emulsion Jet in Crossflow

Considering the relevant fluid properties in the current study provided in Eq. (18), the plume droplet size, represented by the spray Sauter mean diameter (D_{32}), is shown in Eq. (21). The Buckingham π theorem is used to group 17 variables, which include reference dimensions of mass, length, and time into 14 nondimensional groupings. The nondimensional groupings used to determine the normalized relation of D_{32}/d are provided in Eq. (22). The functionally dependent results are the same as those derived in Eq. (19) and are represented as normalized size, length, and forces balances in Eq. (23). The overall form is almost identical to Eq. (20).

$$D_{32} \sim f(d, y, x, \rho_l, \rho_d, \rho_g, U_l, U_g, \mu_l, \mu_g, \sigma_s, \sigma_i, D_{d32}, \Phi, F_D, g), \tag{21}$$

$$\frac{D_{32}}{d} \sim f\left(\frac{y}{d}, \frac{x}{d}, \frac{\rho_l U_l^2}{\rho_g U_g^2}, \frac{\rho_g U_g^2 d}{\sigma_s}, \frac{\mu_l}{\sqrt{\rho_l \sigma_s d}}, \frac{\rho_g U_g d}{\mu_g}, \frac{\rho_l U_l d}{\mu_l}, \frac{D_{d32}}{d}, \Phi, \frac{\sigma_s}{\sigma_i}, \frac{(\rho_l - \rho_g) g d^2}{\sigma_s}, \frac{(\rho_d - \rho_c) g D_{32d}^2}{\sigma_i}, \frac{F_D}{\rho_g U_g^2 d^2}\right), \tag{22}$$

$$\frac{D_{32}}{d} \sim f\left(\frac{y}{d}, \frac{x}{d}, q, \mathrm{We}_{\mathrm{aero}}, \mathrm{Oh}_l, \mathrm{Re}_g, \mathrm{Re}_N, Z, \mathrm{Bo}_{l-g}, \mathrm{Bo}_e, C_D\right). \tag{23}$$

With the framework for describing how an emulsified liquid jet penetrates and atomizes being established, the next step involves carrying out appropriate experiments to allow the functional forms provided above to potentially be reduced to an engineering design guide.

3. APPROACH

3.1 Experimental Facility

The jet in crossflow experiment was conducted on an atmospheric spray test stand. A straight, rectangular test section was used; with dimensions of 10.2 cm (height; y-dir) by 35.6 cm (length; x-dir) by 7.6 cm (width; z-dir). The liquid jet nozzle exits were flush with the test section wall. A photo with data and coordinate axes overlaid is provided in Fig. 4(a). The crossflow air enters from the left of the test section, which is established to

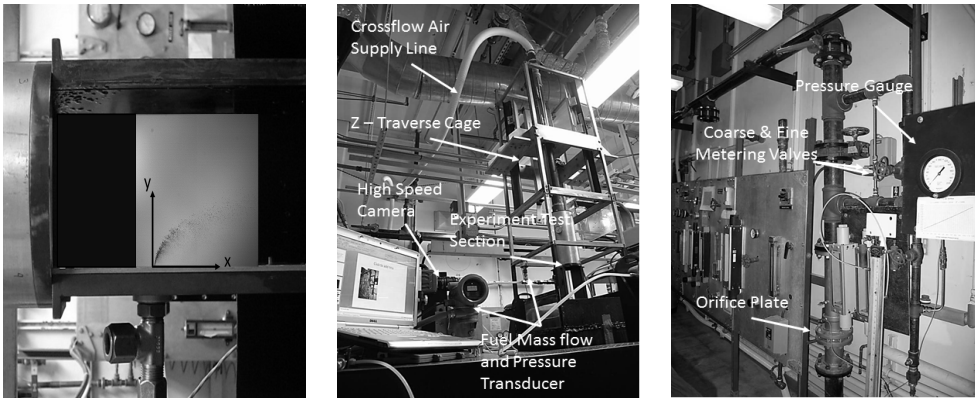

(a) (b) (c)

FIG. 4: Jet-in-crossflow experiment showcasing (a) test section, (b) test rig setup, and (c) crossflow air setup.

be in line with the x-direction. A cylindrical air box provides a large volume to expand the air stream, initially exiting from a 5.0 cm pipe, and then to provide a uniform flow, the flow enters a 2.5 mm gridded mesh, situated 10 in. upstream of the test section [displayed in a vertical orientation in Fig. 4(b)]. The air box consists of an expansion section and a meshed baffle at its entrance, where the air expands to a 12.7 cm diameter flow section upon exit from the baffle. Next, the flow smoothly transitions from a circular flow section to the rectangular test section of interest over a 30.5 cm length to ensure flow uniformity, as documented from flow measurements by Leong et al. (2001). The experimental test section and air box are coupled by a circular-to-rectangular transition piece. Air flow is metered using a critical flow orifice with parallel coarse and fine needle valves and a precision pressure gauge [Fig. 4(c)]. The air flows through a flexible line to the top of the test section, which is all mounted on a three-axis traverse.

The nozzle geometry allowed for fully developed flow to be established upstream of the exit plane. A liquid flow length (L) of 8 mm with a sharp-edged entrance was used. Two nozzle diameters (d), 0.57 mm and 0.72 mm, equating to L/d values of 14.0 and 11.1, respectively, were used during testing.

3.2 Test Liquids

The liquids used in this study are low sulfur distillate #2 (DF2) and filtered water from the tap. The measured fluid properties of these test liquids are provided in Table 1. Surfactants were not used. Rather, emulsions were generated with a low pressure drop ($\sim$1 psi) static mesh mixer following the introduction of each component into a T-junction. The resulting emulsion then flows $\sim$25 cm to the point of injection. To prevent possible coalescence, a second screen filter was placed 3 mm upstream of the final

TABLE 1: Liquid properties (laboratory ambient conditions)

	DF2	**Water**
Chemical Formula	$C_{10-14}H_{20-28}$	H_2O
Density (ρ_l) [kg/m^3]	825	1012
Viscosity (μ_l) [kg/m-s]	2.93E-03	1.37E-03
Surface Tension (σ) [kg/s^2]	0.0280	0.0693
Interfacial Tension (σ_i) [kg/s^2]	0.0268	

contraction into the orifice nozzle or 11 mm from the nozzle exit plane. Discrete water droplet distributions were determined to be in the low limit of macroemulsions (1 to 30 μm range) based on experiments comparing performance from stabilized emulsions and unstable emulsions (Bolszo, 2011; Bolszo et al., 2010).

Three water mass fractions (Φ) were selected: neat DF2 Φ = 0.00, emulsion with Φ = 0.23, and an emulsion with Φ = 0.38. A single liquid flow rate was chosen for each nozzle in order to isolate the influence of the emulsion's effect on the liquid plume. Crossflow air flow rate was varied between three values. The average profile velocity used, which was determined from calculation. The tabulation of the test values utilized in the current work is presented in Table 2. Table 2 presents values for $\dot{\gamma}$ with the current nozzles varied between values of 50,000 s^{-1} and 250,000 s^{-1}. The calculated ranges of nondimensional numbers of interest are also presented in Table 3.

3.3 Diagnostics

A Malvern Real Time Sizer (RTS) laser diffraction instrument with a 450 mm focal length lens was used to measure spray droplet statistics. The 9 mm diameter laser beam was positioned 40 mm downstream from the nozzle exit. Measurements were taken

TABLE 2: Conditions for jet in crossflow test matrix

Nozzle Diameter (d) [mm]	0.57			0.72		
Crossflow Air Velocity, (U_g) [m/s]	44	52	68	44	52	68
Crossflow Mass Flow [kg/min]	24	29	38	24	29	38
Liquid Velocity (U_l) [m/s]	14			18		
Liquid Inject. Pressure (ΔP_l) [MPa]	0.086			0.124		
Liquid Mass Flow [kg/min]	0.12			0.25		
Emulsion Water Mass Fraction (Φ)	0.00	0.23	0.38	0.00	0.23	0.38
Momentum Flux Ratio (q)	27	46	60	44	82	117

TABLE 3: Experimental ranges of nondimensional numbers and physical variables

Momentum Flux Ratio (q)	38	136
Aerodynamic Weber Number ($\mathrm{We}_{\mathrm{aero}}$)	17	145
Gaseous Reynolds Number (Re_g)	1,300	8,400
Nozzle Reynolds Number (Re_N)	1,600	3,300
Liquid Ohnesorge Number (Oh_l)	0.006	0.051
Vertical Distance (y/d)	5	141
Downstream Distance (x/d)	0	70
Nozzle Shear Rate ($\dot{\gamma}$) [s^{-1}]	50,000	250,000

20 mm apart in the vertical direction until the diffraction signal reached a steady value. This region of steady droplet statistics established the measurement location.

High-speed cinematography (Vision Research Phantom 7.2 camera) was utilized to capture videos for jet in crossflow experiments of unstable emulsions. A 2 μs exposure rate was utilized for each frame. The video captured for each case was trimmed to 300 frames sampled from the full frame rate cine file at a rate of 20 frames per second to ensure effective time averaging.

3.4 Image Processing

A Sobel operator which isolates the largest directional gradient from light to dark pixels, allowing emphasis of the spray edge, was selected as most effective in edge distinction. This filter operation was applied to each video and was performed within the Phantom Camera Control software. Penetration was then based on the resulting top edge of the spray plume. The gradient vector edge identified by computing the intensity derivative and the values in the vertical direction were used, any region of constant intensity values was nulled, a procedure described and outlined in image processing texts (Gonzalez et al., 2004). After the Sobel edge vertical filter is applied, each image frame in the video is further processed using Matlab to filter out any noise and interferences that are not relevant to the spray plume. This is done by first converting the frame into a binary image. The Matlab function for conversion to a binary image requires the input of a cutoff intensity value (LEVEL) for which it will only accept pixels of intensity (0–1) above the chosen value and convert them to 1. It is difficult to assign a constant value for "level" for all cases since the variation in water concentration obscuring the backlighting will affect the light luminosity for each image. As a result, a different LEVEL value must be applied to each frame. The level value is chosen using MATRIX's GRAYTHRESH function, which implements Otsu's method to determine a cutoff intensity value. Otsu's method classifies the pixels into either foreground or background pixels and calculates

the optimal threshold value that separates the two classifications by minimizing their variance (Gonzalez et al., 2004; Otsu, 1979). This is then the threshold value used in place of LEVEL. Once 300 frames are converted to binary images they are time averaged into one image as displayed in Fig. 5(a).

To capture the penetration into the crossflow, the next step was to trace the top edge of the spray plume. A Matlab code was developed to map the pixels on a y vs. x plot, tracing the pixels with the highest y coordinate value for every x coordinate. In order for the code to trace the top edge of the plume, the image is converted to binary again so that all pixels regardless of value are given a value of 1. This allows the code to simply trace the pixels with the highest y coordinate using a programming loop as displayed in Fig. 5(b).

A few white pixels or regions of pixels (attributed to rogue droplets, noise, or instrument error) are noted away from the main spray plume represent outlying or nonphysical features in the trajectory. Although these points demonstrate that liquid droplets exist outside of the spray plume area, they interfere with the desired smooth trace of the plume edge as shown in Fig. 5. To mitigate interference by these white pixels, Matlab's "BWAREAOPEN" function was utilized. This function removes clusters of pixels that are connected in groups of less than a given integer. An integer value of 200 was visually determined as a sufficient value to discriminate unnecessary pixels and isolate the dominant morphology in the trajectory arch. Application of this function removes the unwanted spots from Fig. 5(a), but does not remove any connected features, which defines the boundary of interest for the trace, and is demonstrated in Fig. 5(b). The boundary determined binary fields, which have been treated for enhanced upper edge detection, intensity, and morphology thresholding are now traced on the top surface along every x pixel, as is distinguished by the darkened line overlaid on the spray boundary. This re-

(a) (b) (c)

FIG. 5: (a) Time-averaged image, (b) binary image of emulsion case with Φ = 0.23, q = 52, and (c) trace of morphology processed plume.

sultant traced line was utilized as a representative trajectory for each jet in the crossflow test case and further penetration analysis in Fig. 5(c).

4. RESULTS

4.1 Discharge Coefficients and Breakup Regimes

The orifice nozzle discharge coefficient (C_d) for the two nozzles, defined in Eq. (24), was measured over the laminar range at a given nozzle Reynolds number ($\mathrm{Re}_N = \rho_l U_l d/\mu_l$). The results are provided in Fig. 6. In the current test, Re_N varied between two target values of 1600 and 3300 for neat DF2 (Φ = 0.00), which corresponds to an injector C_d varying from 0.65 to 0.70 for the 0.72 mm and 0.57 mm diameter nozzles.

$$C_d = \frac{\dot{m}_l}{A_o\sqrt{2\rho_l \Delta P_l}}, \tag{24}$$

To establish the expected breakup mode for the conditions studied, the current test cases are plotted on a q versus $\mathrm{We}_{\mathrm{aero}}$ regime map (Wu et al., 1998) in Fig. 7, which indicates a difference in dominant breakup behavior between the neat and emulsion cases.

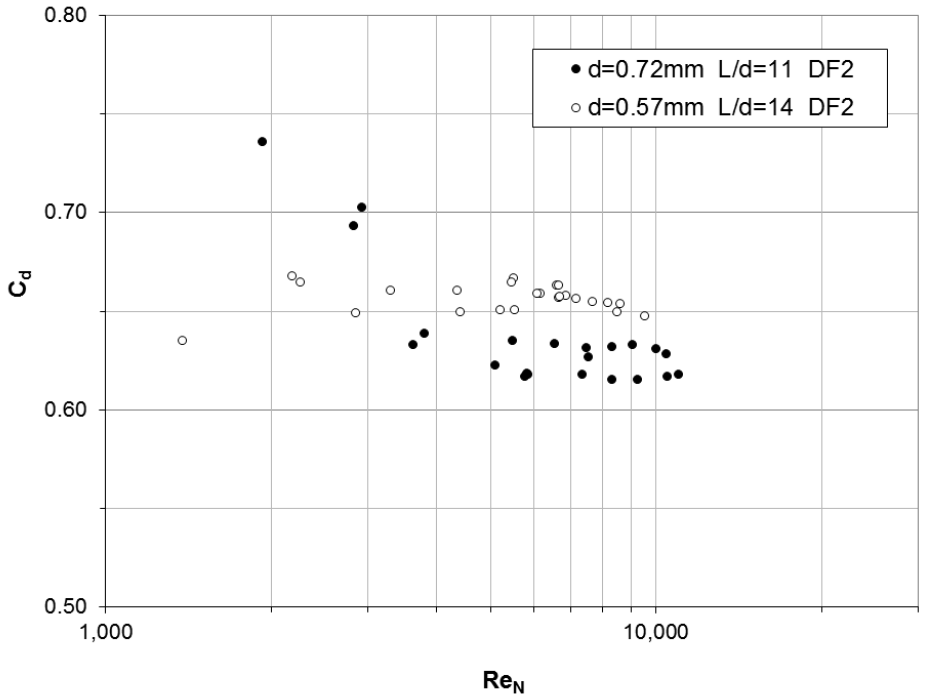

FIG. 6: C_d vs. Re_N from laminar to turbulent flow.

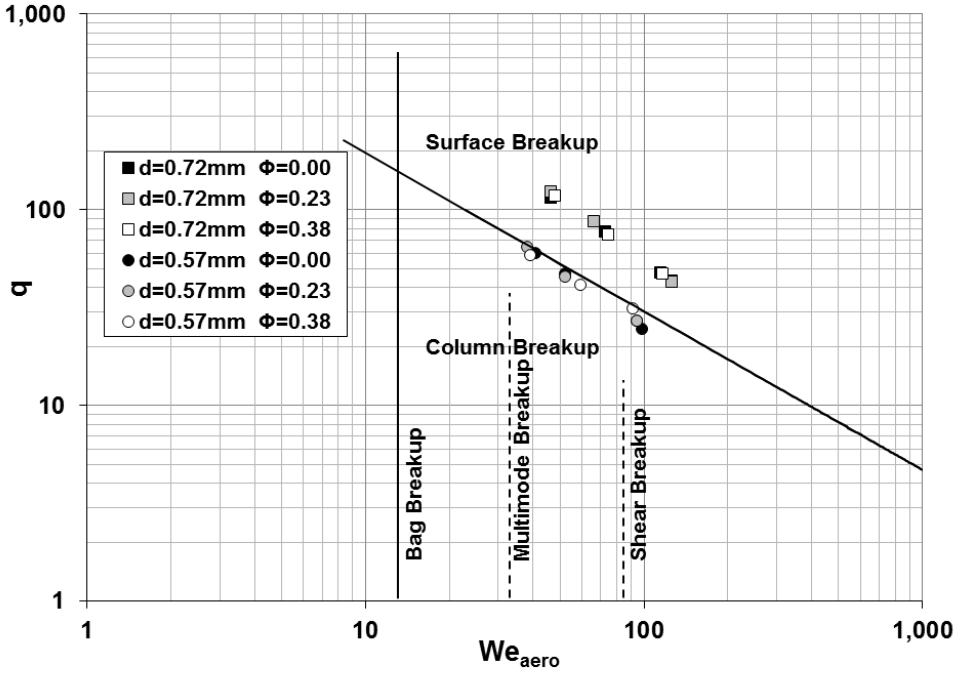

FIG. 7: q vs. $\mathrm{We}_{\mathrm{aero}}$ regime plot for current test cases.

The difference between the two regimes (resulting from use of emulsion vs. neat liquids) can also be observed in images, as illustrated in Table 4.

As shown in Table 4, larger numbers of droplets are produced from surface stripping at higher versus lower q values. However, it is also observed that a smaller number of fine droplets are produced when significant amounts of water are added to form an emulsion (varying Φ) for a given case, consistent with the different regimes suggested by Fig. 7.

4.2 Penetration Behavior

Resultant edge enhanced, averaged exposures utilizing 300 images in comparison to one 2 μs exposure is provided in a side-by-side comparison in Fig. 8. In comparing the averaged cases, the difference between the intensity was of prime interest in assessing a representative exposure for line boundary determination in distinguishing from backlighting or background intensity gradients.

The methodology described above was used to establish the plume trajectory. Table 5 summarizes the average intensity cutoff values in distinguishing between a black (0) and white (1) pixel color (value) in binary. Also provided is the standard deviation in averaged lighting value in determining the intensity threshold for 300 exposures. With

TABLE 4: Single high speed exposure of DF2 and emulsions

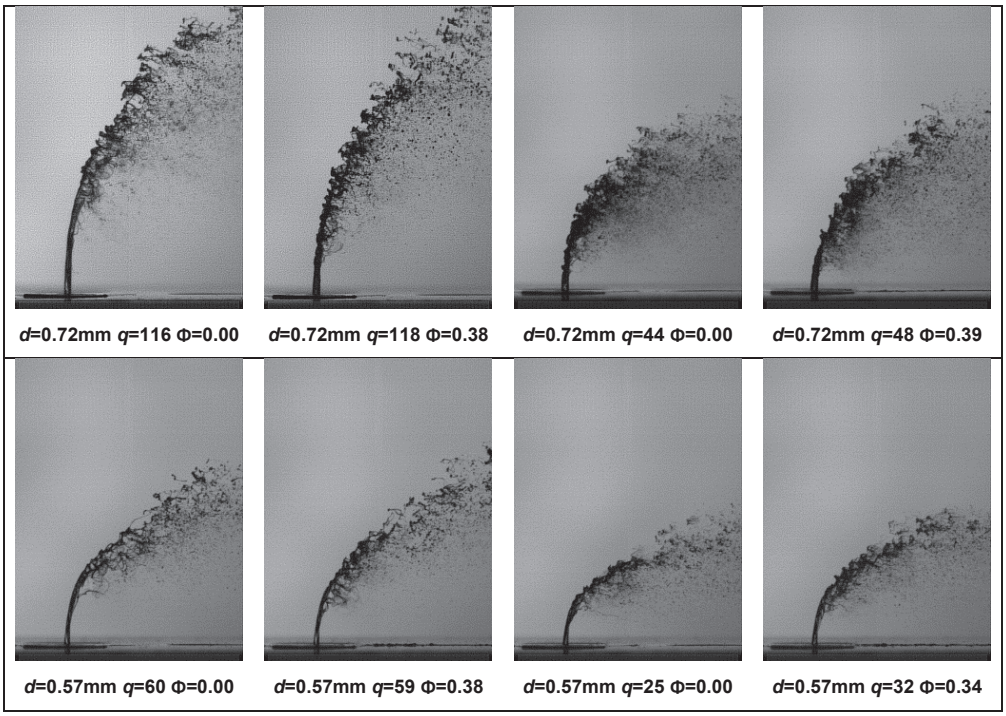

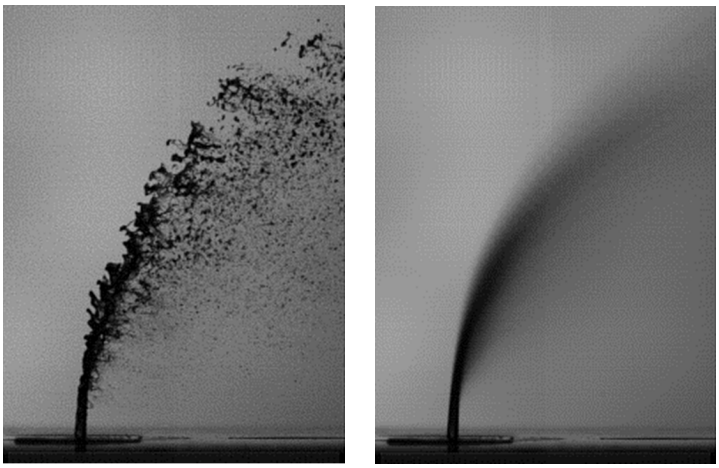

(a) (b)

FIG. 8: (a) High-speed exposure and (b) example 300 exposure average of test case used for determining plume trajectory (d = 0.57 mm, q = 46, Φ = 0.24).

TABLE 5: Intensity threshold values from Otsu's method

Flow Conditions			Intensity Threshold	
d (mm)	Φ (0 – 1)	q ( )	Ave. (0 – 1)	StDev. (0 – 1)
0.72	0.00	116	0.290	0.011
0.72	0.22	125	0.298	0.012
0.72	0.38	118	0.290	0.011
0.72	0.00	78	0.272	0.011
0.72	0.22	88	0.281	0.012
0.72	0.36	75	0.272	0.011
0.72	0.00	48	0.246	0.015
0.72	0.00	44	0.182	0.016
0.72	0.24	43	0.248	0.015
0.72	0.39	48	0.257	0.014
0.57	0.00	60	0.331	0.007
0.57	0.23	65	0.316	0.007
0.57	0.38	59	0.325	0.009
0.57	0.00	47	0.299	0.009
0.57	0.24	46	0.280	0.008
0.57	0.38	41	0.296	0.008
0.57	0.00	25	0.243	0.014
0.57	0.22	27	0.252	0.014
0.57	0.22	27	0.243	0.015
0.57	0.34	32	0.254	0.011

the exception of one case at d = 0.72 mm, Φ = 0.00, and q = 44, the average threshold intensity was consistently very near 0.3 and a standard deviation of $\pm$0.01. Spread in data was observed, and is due to differences in mean image intensity within the video frame based on overall light obscuration from the liquid. The larger the dispersion of the spray plume, the lower the amount of light which is able to reach the aperture, reducing the overall contrast of the picture. This loss in overall exposure clarity makes distinguishing the trajectory edge more difficult farther downstream. The effect of nozzle size or internal geometry (L/d) is also believed to contribute to the transition of the flow to turbulence and of the growth of surface instabilities, which is used to explain the slight groupings by nozzle size noticed between the normalized data sets.

The trajectories from the processed images of neat DF2 for three general q values are provided in Fig. 9. For each case, the trajectory is monotonically increasing with q (increase in liquid versus gas) except for the 0.72 mm diameter, q = 116 case which has a trajectory close to the higher air flow case with q = 78.

Figure 10 presents the trajectories for emulsions. The trend in trajectory at a given Φ ($\sim$0.23 or $\sim$0.38) demonstrates a strong direct proportionality with q for a given nozzle diameter. However, when comparing the data for a given q value, it correlates to the dominant factor responsible for the trajectory height. The evidence of this is clear when comparing the effect of Φ (from 0.00 to 0.38) on the trajectory height in Fig. 9 versus Fig. 10. This comparison shows that for a trajectory height at a given q, increasing Φ will increase the overall trajectory.

Isolating the fluid variables of the current emulsion results in a familiar nondimensional combination of governing parameters that has already been reported in the literature. As a first step, correlations for neat DF2 (Φ = 0.00) were considered and the Buckingham π results are used as a foundation for further derivation [Eq. (20)]. Simplification of Eq. (20) to the forms of Eqs. (5)–(9), presented in Eq. (25), were considered for penetration trends in the current data. Yet, of all the correlations considered, the basic form presented by Geery and Margetts (1969) and used by Wu and co-workers (1998) [Eq. (5)] provided consistently the best fit to the current data set. Surprisingly,

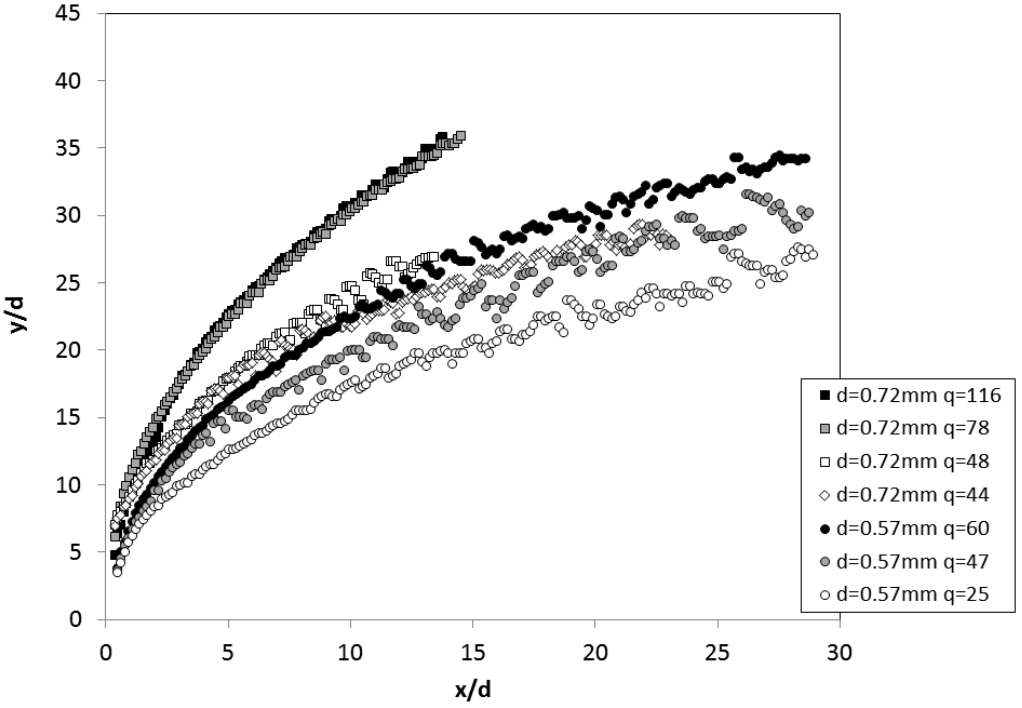

FIG. 9: DF2 jet edge trajectory for two d = 0.57 and 0.72 mm orifices.

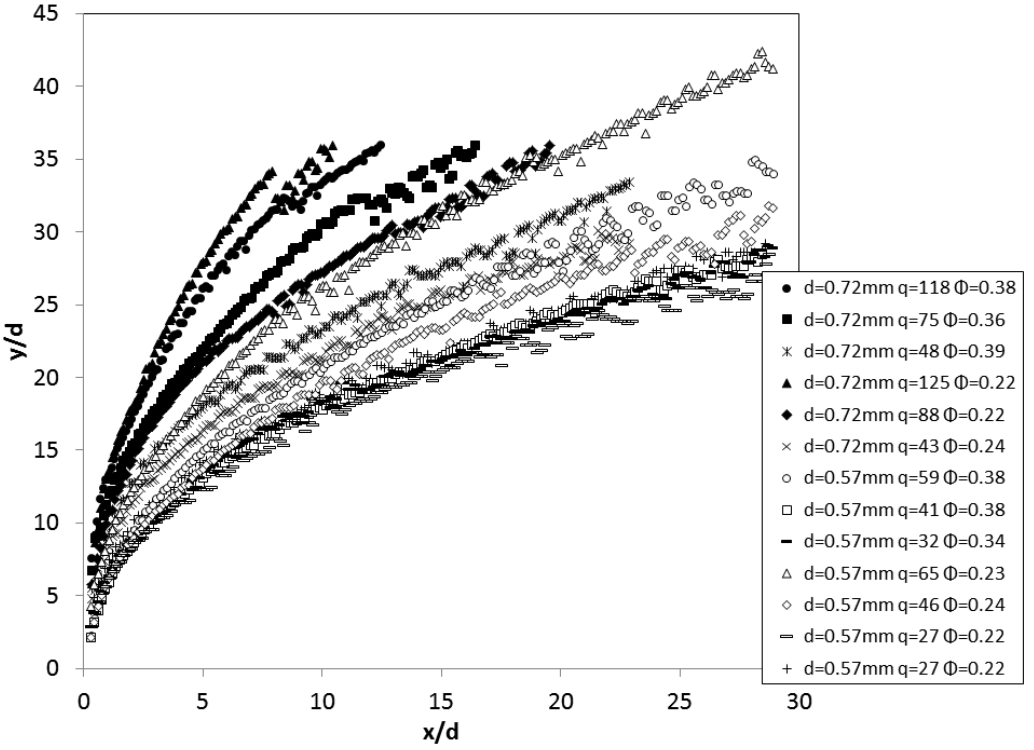

FIG. 10: Emulsion jet edge trajectory for two 0.57 and 0.72 mm orifices.

many of the factors in Eq. (20) demonstrated very small dependences with the given data. A linearization of the penetration equations was performed by taking the natural log of both sides of Eqs. (5)–(9). The Re_g, Re_l, $\mathrm{We}_{\mathrm{aero}}$, $\mathrm{Oh}_{l,}$ and the viscosity term as reported by Stenzler et al. (2003) and Birouk et al. (2007) did not improve the fit within a +0.02 goodness-of-fit R^2 value, while concurrently improving the orientation of the linear slope with a further improved degree precision than 1.001 compared with the values already attained simply from the Wu et al. equation [Eq. (5)]. Both Bond numbers in Eq. (25) did not improve the fit, revealing that the effect of the body forces is handled by the emulsion liquid density versus the component density. Each of these additional nondimensional terms did not collapse the spread closer to the one-to-one correlation line. The goodness-of-fit is displayed as a linear least-squares regression fit R^2 value and slope with the exponential taken of both sides to put the equation back into its nonlinear form and then plotted to demonstrate its correlation potential. One question to consider is whether the discharge coefficient of the orifices contributes to the measured variation. Work by Brown et al. (2007) demonstrated the collapse of multiple jet in crossflow data sets is possible when considering the nozzle effective area by incorporating C_d. The result in the current work also provided a con-

sistent improvement in the correlation for each case. This improved fit is demonstrated by an improved regression R^2 from 0.92819 to 0.94257 for DF2 trajectory cases. In the present results, the C_d did not vary substantially among the cases, but including it did improve the correlation. The coefficients that provided this best fit were a = 1.893, b = 0.3817, and c = 0.4196. While the C_d between the cases did not vary substantially, inclusion of the C_d results in a substantial increase in q, which illustrates the need to clearly specify the basis for the values of q used (i.e, based on C_d = 1 or measured C_d).

$$\frac{y}{d} \sim f\left(\frac{x}{d}, q, \mathrm{We}_{\mathrm{aero}}, \mathrm{Re}_g, Z, \mathrm{Bo}_{l-g}, \mathrm{Bo}_e, C_D\right). \tag{25}$$

In further consideration of previous correlations, it is noted that the effect of liquid viscosity [Eq. (8)], $\mathrm{We}_{\mathrm{aero}}$ [Eq. (7)], and Re_N were all evaluated in the present work and did not show a significant improvement in overall predictive fit. Of particular interest with emulsions was the increased viscosities due to additional interfacial forces present (Bolszo, 2011; Bolszo et al., 2010). However, this viscosity effect was not shown to be a significant governing variable in impacting the emulsion trajectory.

To further isolate the relative behavior of emulsions and neat liquids, results for emulsions alone were compared with pure oil (DF2) in Fig. 11. Interestingly, inclusion of the emulsion data did not affect the regression fit, which maintained a unity slope and an R^2 = 0.9424. The trend in increasing trajectory with increasing Φ presented in Fig. 10 is therefore explained and sufficiently accounted for by the increase in density from the water addition within the DF2 for the emulsion. Past analyses have identified that the emulsion fluid properties can be represented as deviations from Newtonian flow behavior found for the continuous liquid (DF2) (Bolszo et al., 2010).

Examining the coefficient values for b = 0.4352 and c = 0.4342 in Eq. (26), it is evident that the equation can be simplified to single exponent of 0.43 without any significant loss of fit, resulting in Eq. (27):

$$\frac{y}{d} = 1.4811 q^{0.4352} \left(\frac{x}{d}\right)^{0.4342}, \tag{26}$$

$$\frac{y}{d} = 1.48 \left(q\frac{x}{d}\right)^{0.43}. \tag{27}$$

Careful inspection of the results shown in Figs. 9–12 does suggest some classification as a function of injector diameter. However, recalling that that the two injector diameters result in differing dominant breakup regimes (Fig. 7), it is hypothesized that this variation in penetration is due to the role of breakup type (Fig. 3). This suggests that different penetration correlations for different regimes may further improve the fit to the current data. However, from an engineering perspective, the improvement may not be substantial. The spread in data shown in Fig. 11 and Fig. 12, as mentioned earlier, is due to differences in mean image intensity within the video frame based on overall light obscuration from the liquid.

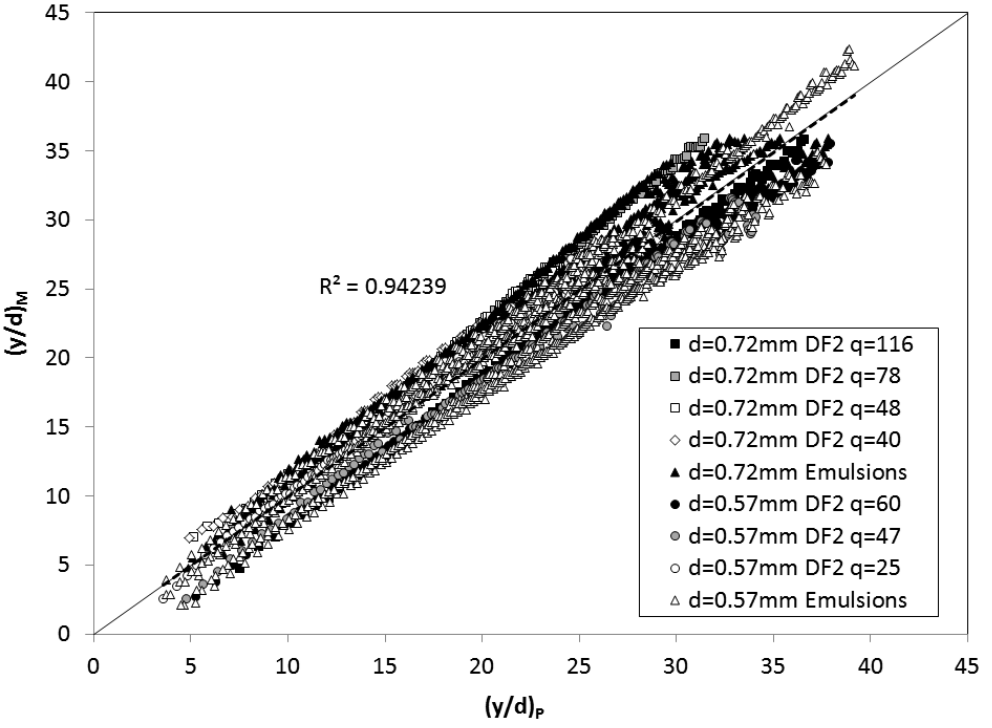

FIG. 11: Jet edge trajectory measured vs. general correlation (C_d = 0.65 – 0.70) for DF2 and emulsions.

Revisiting the original collection of nondimensional groupings in Eq. (19), the current analysis reveals that only 3 of the 13 terms are needed to establish a very good fit for emulsions. Additional terms do not improve the overall fit between emulsions and neat fuels for the conditions studied, which implies that the results are within the experimental error. With the moderate $\mathrm{We}_{\mathrm{aero}}$ values considered, no perceivable influence was observed beyond that of q. Stenzler and co-workers indicated a small $\mathrm{We}_{\mathrm{aero}}$ dependency (exponent of –0.088) for a range of values from 2.5 to 141 (Stenzler et al., 2003). In the current work, the effect of viscosity was also not observed to produce an improved fit. In comparison, Stenzler and co-workers (2003) and Birouk and co-workers (2007) suggested weak dependencies upon viscosity, yet indicate disagreement in the sign of influence, with an exponent of –0.027 and +0.079. In the present work, while viscosity increases substantially for the emulsion, a correction of fit was not identified through an Oh_l, $\mathrm{Re}_{l,}$ or relative viscosity ratio.

In summary, a rigorous approach to development of a penetration correlation for an emulsified liquid jet in crossflow has been implemented and evaluated with new data. Interestingly, the original correlations from Geery and Margetts (1969) and results from Wu and co-workers (1998), Eq. (5), was found to sufficiently describe the penetration

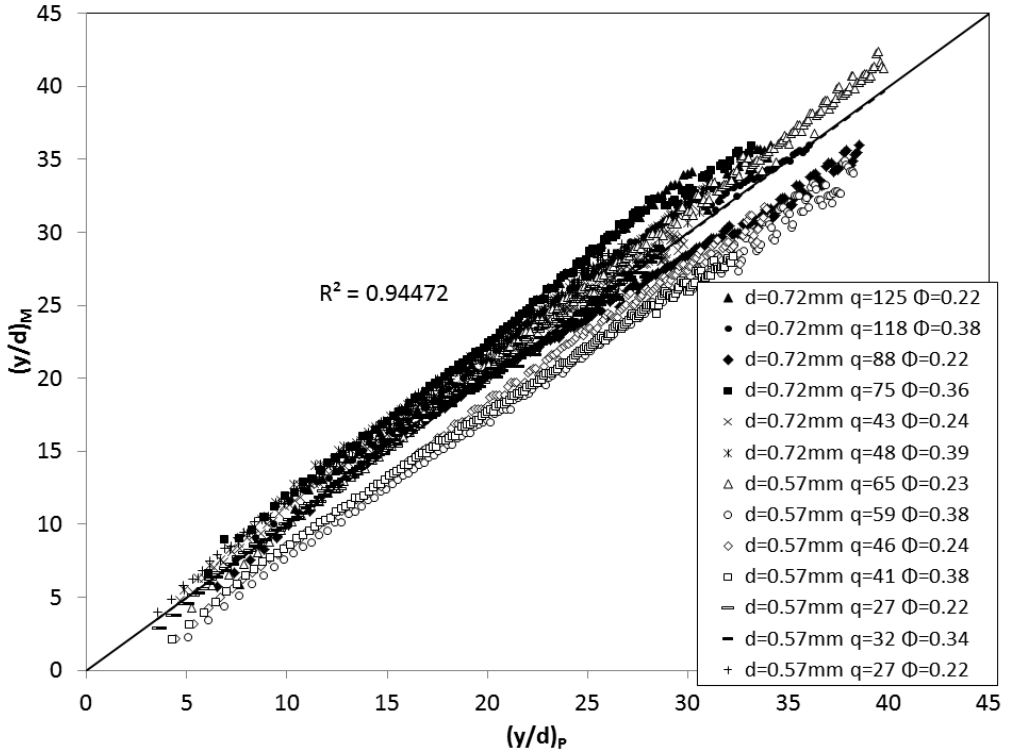

FIG. 12: Jet edge trajectory measured vs. corrected general correlation (C_d = 0.65 – 0.70) for emulsions.

of the far edge of the jet. The emulsion momentum flux and density are shown to be the primary fluid properties responsible for determining the jet trajectory height statistically and is represented by Eq. (27). Despite the apparent complexities associated with the emulsion, the contribution of the terms associated with these complexities contributed little compared to the momentum flux ratio.

4.3 Droplet Size Measurements

The droplet sizes generated by the atomization of the jet in the crossflow are now discussed. A downstream position of x = 40 mm was selected in order to ensure measurements were obtained within a region of the spray plume with spherical droplets rather than intact jet or large ligaments. Measurements commenced 15 mm away from the wall to mitigate vignetting of the scattered light by the wall. Measurements were taken at 12 mm spacing increments in the y direction until insignificant numbers of drops were detected (less than 20 of the 60 1-Hz measurements generated significant signal). It is of primary interest to evaluate the difference in droplet size between the pure oil and their

combination as a water-in-oil emulsion. Results are provided for the 0.57 mm nozzle in Fig. 13 and the 0.72 mm nozzle in Fig. 14. In both figures, the emulsions produce larger droplet size distribution D_{32} values away from the wall for all cases. The increase in size in both figures is noted as monotonically increasing when comparing with Φ at a fixed q value (larger droplets are positioned farther on the abscissa). This increase in size with Φ is most apparent at the highest ordinate values (the highest vertical values measured in the plume). In the near-wall region, multiple cases which have similar D_{32} values (possibly smaller for the high q cases for the 0.57 mm nozzle in Fig. 13) are observed for both neat DF2 and emulsions.

To provide a complete data set, the droplet size results for pure water are also provided in Fig. 15. These data are used to establish a baseline relationship for the phenomenological forces involved when emulsions are used. The observed deviation in droplet size results between the pure liquids and the emulsions is now investigated in greater detail.

In Table 6 and Table 7, the measured droplet histograms are provided for all the pure fuel oil, pure water, and emulsion cases at high and low q to reinforce the D_{32} values provided. For each plot within, the difference in the droplet distribution in vertical

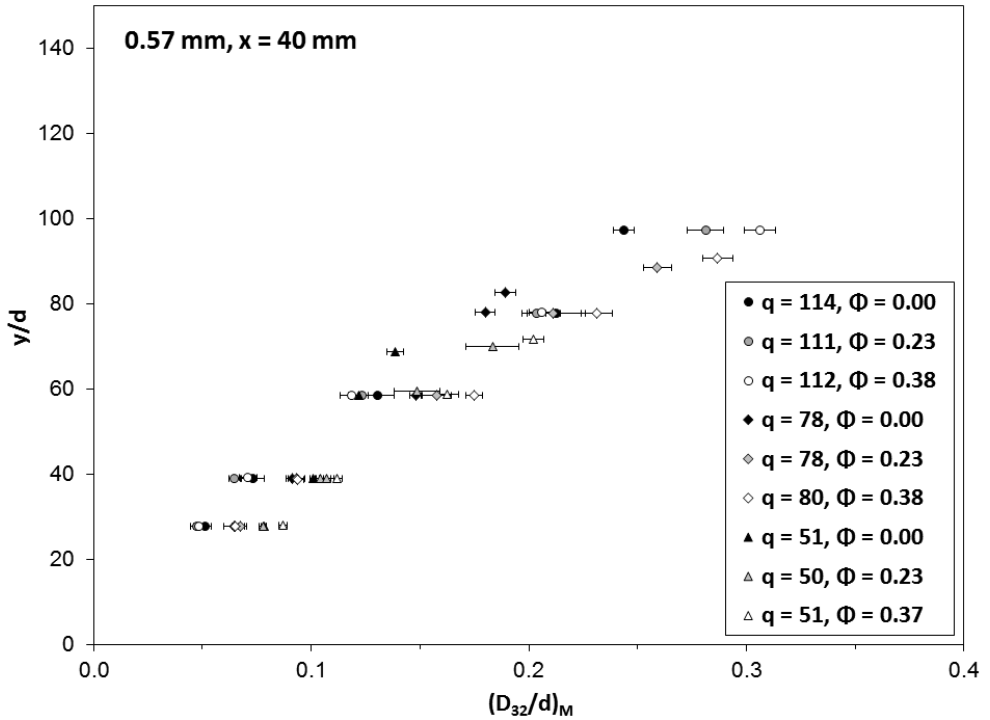

FIG. 13: Laser diffraction D32 plotted as a function of normalized vertical trajectory distance y for 0.57 mm nozzle.

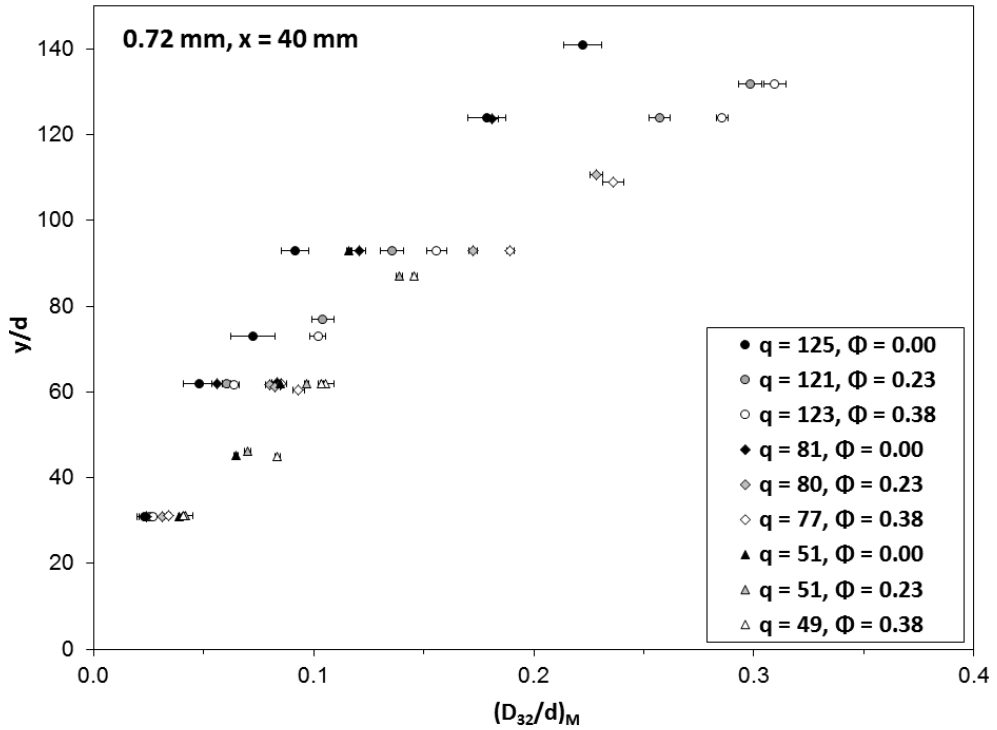

FIG. 14: Laser diffraction D32 plotted as a function of normalized vertical trajectory distance y for 0.72 mm nozzle.

distance is provided for both nozzle diameters. Note that, for most cases, the overall shift in distribution with water addition is very similar between both nozzles. The most significant distinction between the nozzles is what occurs at locations farthest from the injector wall; specifically, a wider distribution occurs for the 0.72 mm nozzle cases versus a narrower peak with the 0.57 mm cases. This distinction may be due to a difference in concentration of liquid within the plume, producing a different liquid Reynolds numbers between the two nozzles. When comparing the pure liquid results (Φ = 0.00, 1.00) to the emulsion cases with Tables 6 and 7, the overall distributions are shown to be surprisingly similar in overall size distribution (vertically). It is of interest to now quantify the differences by correlating them to fundamental physical quantities.

Kihm et al. provided a physical–empirical formulation for the determination of the jet in crossflow droplet size within the spray plume for pure liquids using the Buckingham π approach (Kihm et al., 1995). In the present work, this approach was adapted to incorporate the additional factors associated with emulsions while retaining the application to pure fuels.

Evaluating the possible physical nondimensional groupings from spray fluid properties for a round jet orifice, the Buckingham π approach is again undertaken to determine

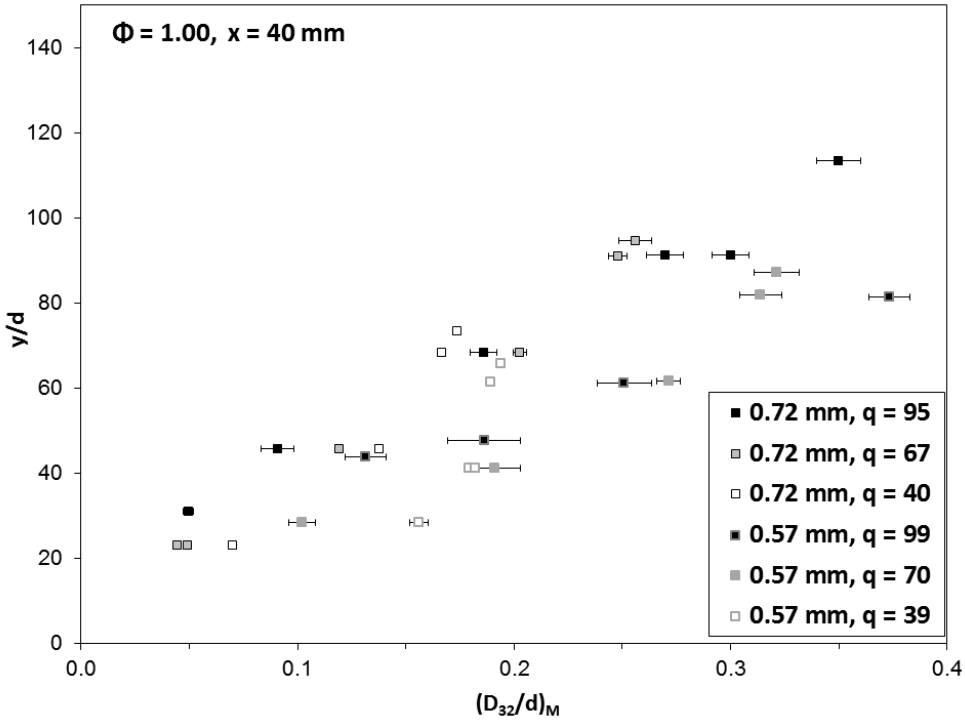

FIG. 15: Laser diffraction D32 plotted as a function of normalized vertical trajectory distance y for water cases.

the jet in crossflow droplet size. Lee and co-workers reported on the phenomenological properties for a high Reynolds number subsonic crossflow; the Re_N is shown to be the dominant breakup mechanism due to turbulent eddies near the liquid surface (Lee et al., 2007). The current investigation produces nonturbulent Re_N from 1300 to 8400 and, from the current statistical regression analysis, was not shown to produce a primary governing effect. To point out an additional significance of the current study, the liquid Weber number ($\mathrm{We}_l = \rho_l U_l d/\sigma_l$) was not considered directly, but was represented by the contributions of both q and $\mathrm{We}_{\mathrm{aero}}$ dimensionally as an approach to relate the prior findings in the jet in crossflow penetration (Sec. 4.2). This simplification was performed in order to isolate the effect of the emulsion on jet breakup. This isolation was done to allow the overall breakup to be cast in terms of a sequence of dependent processes: (1) jet penetration, (2) liquid breakup, and (3) the resultant droplet size distribution formation. Restating the fluid factors and their nondimensional groups in Eqs. (21′) and (23′), the physical relationship is now developed for determining the droplet size dependence across the plume for pure fuels and then for emulsions.

$$D_{32} \sim f(d, y, x, \rho_l, \rho_d, \rho_g, U_l, U_g, \mu_l, \mu_g, \sigma_s, \sigma_i, D_{d32}, \Phi, F_D, g), \qquad (21')$$

TABLE 6: Measured DF2 and emulsion jet in crossflow droplet size distributions within the plume at high q for 0.57 mm and 0.72 mm nozzles at x = 40 mm downstream

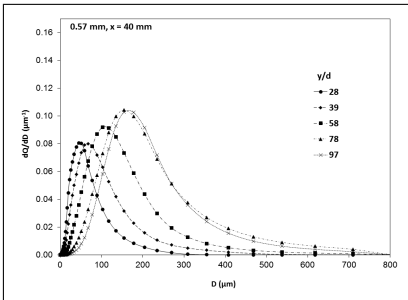	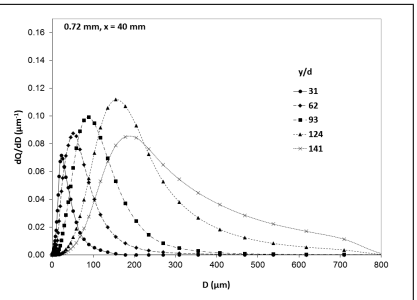
d = 0.57 mm, q = 125, Φ = 0.00	d = 0.72 mm, q = 114, Φ = 0.00
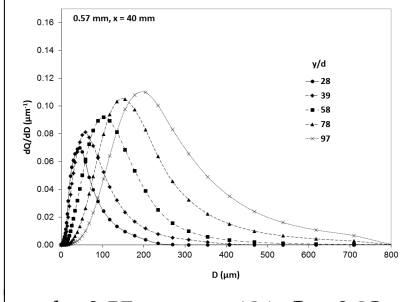	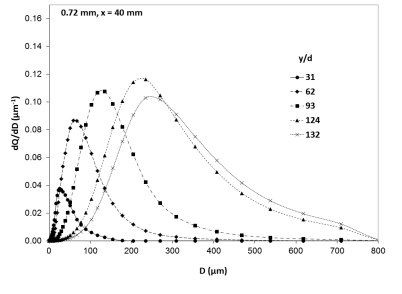
d = 0.57 mm, q = 121, Φ = 0.23	d = 0.72 mm, q = 111, Φ = 0.23
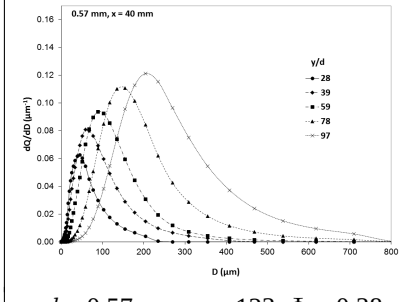	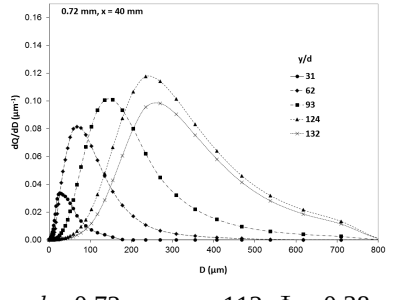
d = 0.57 mm, q = 123, Φ = 0.38	d = 0.72 mm, q = 112, Φ = 0.38
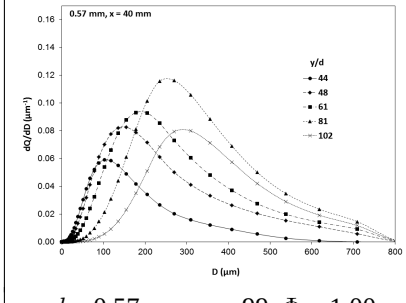	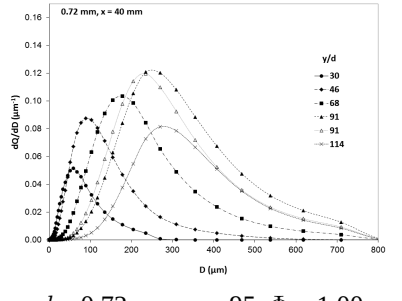
d = 0.57 mm, q = 99, Φ = 1.00	d = 0.72 mm, q = 95, Φ = 1.00

TABLE 7: Measured DF2 and emulsion jet in crossflow droplet size distributions within the plume at low q for 0.57 mm and 0.72 mm nozzles at x = 40 mm downstream

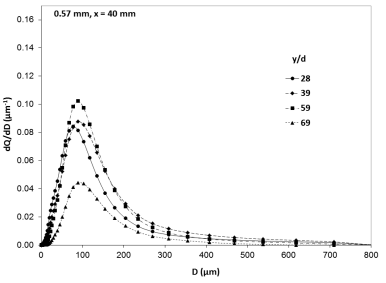 d = 0.57 mm, q = 51, Φ = 0.00	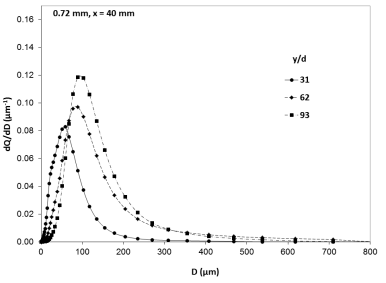 d = 0.72 mm, q = 51, Φ = 0.00
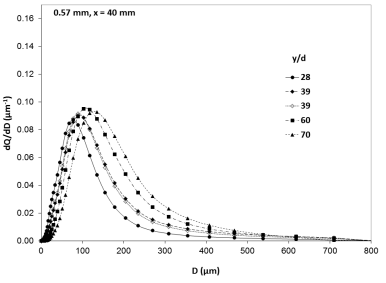 d = 0.57 mm, q = 51, Φ = 0.23	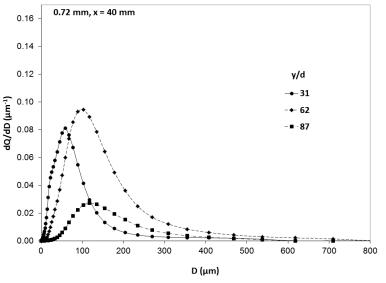 d = 0.72 mm, q = 50, Φ = 0.23
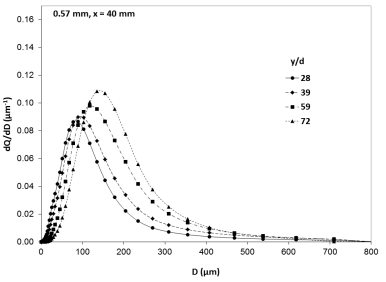 d = 0.57 mm, q = 49, Φ = 0.38	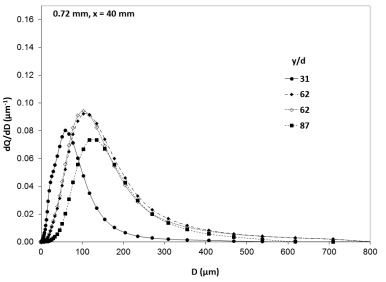 d = 0.72 mm, q = 51, Φ = 0.37
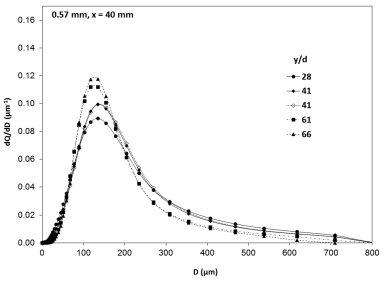 d = 0.57 mm, q = 39, Φ = 1.00	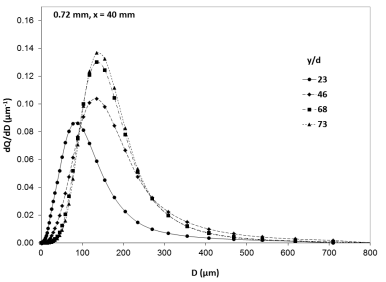 d = 0.72 mm, q = 40, Φ = 1.00

$$\frac{D_{32}}{d} \sim f\left(\frac{y}{d}, \frac{x}{d}, q, \mathrm{We}_{\mathrm{aero}}, \mathrm{Oh}_l, \mathrm{Re}_g, \mathrm{Re}_N, C_D, Z, \mathrm{Bo}_{l-g}, \mathrm{Bo}_e\right). \tag{23'}$$

Considering that the total liquid mass flow is not varied for each of the two nozzles, and data were only taken at a single axial position (x = 40 mm), x/d will not be considered in the overall relation. Further, a very large air-emulsion Bo_{l-g} (1×10^5) suggests body forces dominate the bulk jet–air interaction, while a small Bo_e (1×10^{-8}) suggests interfacial forces dominate within the emulsion. This suggests that the bulk jet movement is dominated by the liquid momentum it is composed of versus the surface tension of the continuous component. Internally, the emulsion experiences strong interfacial forces which repel the components on the same order of magnitude which the surface tension holds the column together. Both these force mechanisms contribute to the resultant breakup and will be considered. The drag coefficient C_D has been reported to vary from roughly 3 to 10 depending on the dominance of their respective breakup modes according to theory (Sallan et al., 2004). If only the shear and multi-breakup modes were considered, C_D should vary only slightly, roughly from values of 3 to 4. Considering the equation form from the findings of Lee et al. (2007) in Eq. (9), C_D correlates inversely to the 1/2 power with trajectory, attributing to a small effect in the current case, which leaves eight usable groupings in Eq. (30). For the pure liquid initially considered, the interfacial forces (S) term and the Bond numbers for respective component's body forces are eliminated. Analysis indicates that the liquid friction force variation (Oh_l) contributes weakly to the expression (a best-fit exponent value of 0.1 was observed). As a result, a single term equation for pure liquids of oil and water is achieved in Eq. (31). Incorporating the current droplet size data and taking the natural log of both sides of Eq. (31), a linear regression was performed on the pure fluids, resulting in Eq. (32), which fits the data with a linear slope of 1.00008 and an R^2 = 0.92893, shown in Fig. 16. Presenting the resultant relation on a nonlogarithmic scale for an exponential comparison of predicted [Eq. (32)] and measured results, is shown in Fig. 17, with experimental standard deviation overlaid. Some residual scatter is noted for the largest droplet diameters, above 150 μm. The raw unaveraged data indicate occasional large droplets at the largest y positions. The combination of the effect these droplets have on the overall D_{32} statistics and the overall lower signal of diffracted light contribute to larger variability in the measurements. The overall dimensional relationships between the exponents all appear well-behaved and contribute at similar order of magnitudes as well as overall contributions that agree with overall sign (+ or –).

$$\frac{D_{32}}{d} \sim f\left(\frac{y}{d}, q, \mathrm{We}_{\mathrm{aero}}, \mathrm{Oh}_l, \mathrm{Re}_g, \mathrm{Bo}_{l-g}, \mathrm{Bo}_e, Z\right), \tag{28}$$

$$\frac{D_{32}}{d} = A\left(\frac{y}{d}\right)^B q^C \mathrm{We}_{\mathrm{aero}}^D \mathrm{Re}_g^E, \tag{29}$$

$$\frac{D_{32}}{d} = 9.33 \times 10^7 \left(\frac{y}{d}\right)^{1.173} q^{-1.711} \mathrm{Re}_g^{-2.087} \mathrm{We}_{\mathrm{aero}}^{-0.419}. \tag{30}$$

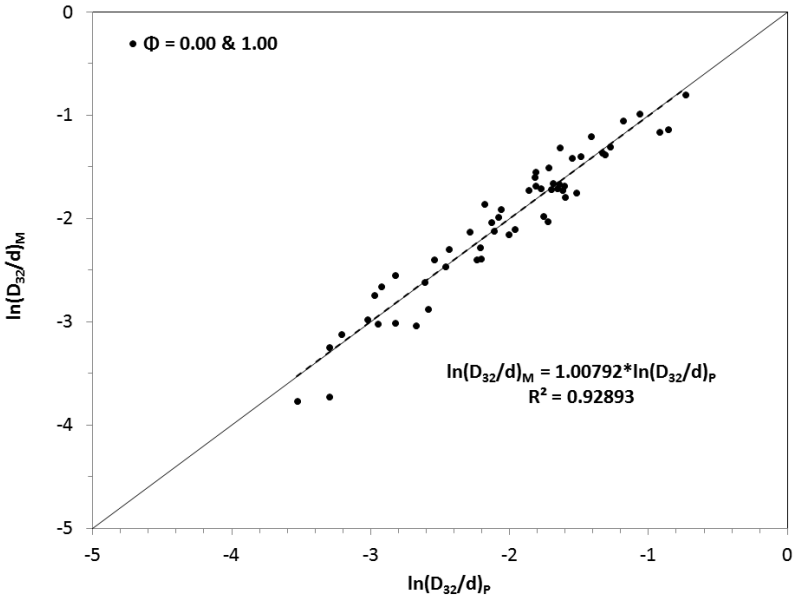

FIG. 16: Linearized measured jet in crossflow droplet size versus correlated droplet size for pure fuels using Eq. (30) and corresponding goodness-of-fit parameters.

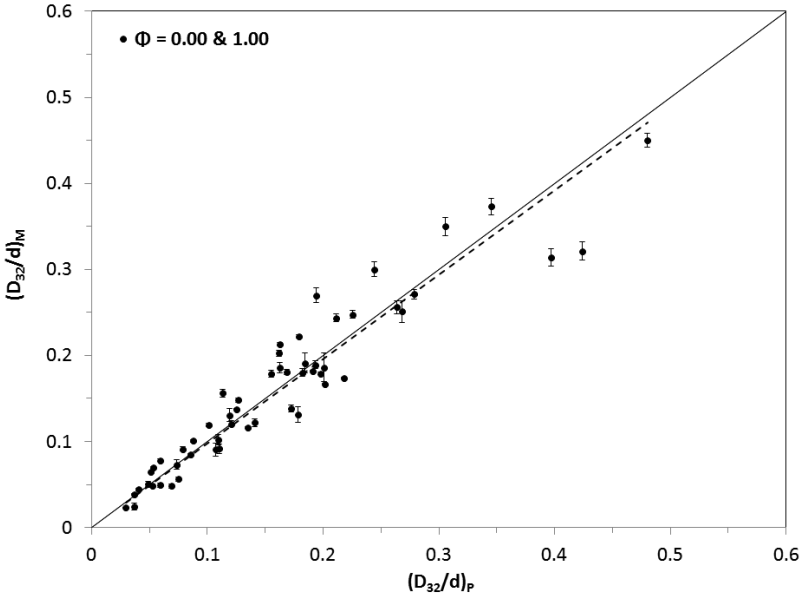

FIG. 17: Measured jet in crossflow droplet size versus correlated droplet size for pure fuels using Eq. 30.

It is now of interest to evaluate how the emulsion cases fit with the current data. The emulsion data are correlated with Eq. (32) and shown in Fig. 18. A significant divergence is observed for the larger droplet sizes. This divergence in droplet size suggests that the emulsion jet break time differs from the pure liquid, resulting in differences at the largest vertical distances. Based on high speed images, an earlier break point of the jet column is noted as it enters the crossflow, which is due to the additional interfacial tension. The presence and size of the dispersed phase within the spray plays a large role in the resulting spray plume droplet distribution. This can lead to larger sporadically released "rogue" droplets from the jet at the highest trajectories. These droplets would not be accounted for in the current penetration analysis due to the time averaging of the high-speed images.

4.4 Development of Interfacial Tension Term for Emulsions

Considering the observed differences in breakup between the pure fuels and their combination as an emulsion in Fig. 18, additional considerations appear necessary to further collapse the results. The difference in body force between the components appears to contribute to a vertical spreading of the overall plume height. As the jet is bent by the

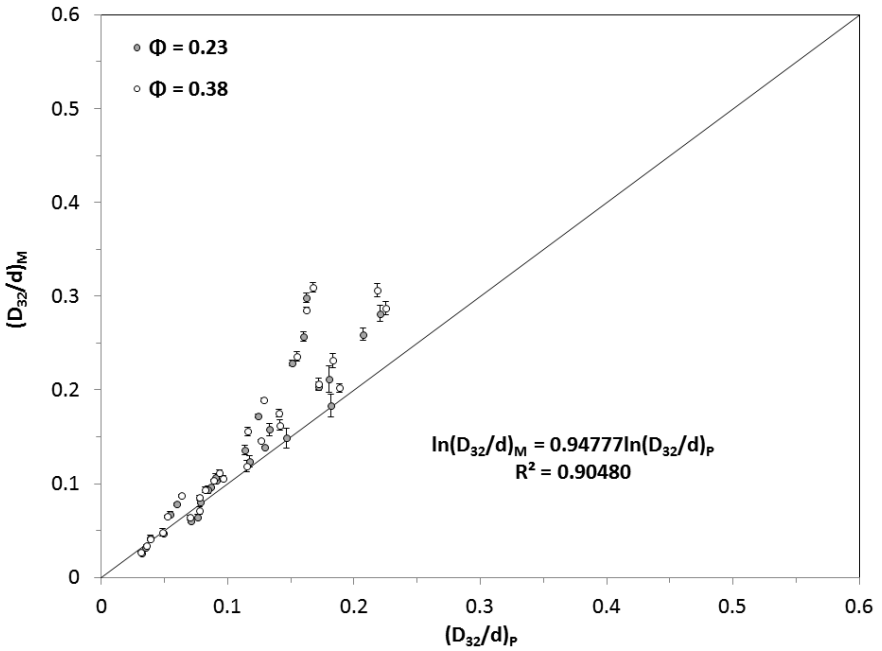

FIG. 18: Emulsion cases correlated using the relationship developed for pure liquids [Eq. (30)].

air's momentum, arching back, denser regions of fuel with higher momentum possess higher trajectories. These components must overcome the jet surface tension in order to break off from the jet. Further, the emulsion jet in crossflow possesses a repulsive interfacial tension in addition to the cohesive forces due to the surface tension of the column, resulting in earlier pinch-off of the column, which allows trajectories to reach even higher values. These two forces counteract each other and are proposed to act at different length scales. Specifically the surface tension acts on the column, represented by the nozzle circumference (or diameter d), whereas the interfacial tension acts along the circumference of the discrete droplet (droplet diameter), represented here by the Sauter mean diameter (D_{32d}).

Formulating the Bond number to represent the breakup of emulsions requires two force balances: (1) between the bulk liquid and the air and (2) between the component liquids. These are formulated below in Eqs. (33) and (34). Note the air density is dropped due to already being considered in the Re_g term in Eq. (32) and only the emulsion density remains. Here the surface tension of the emulsion is that of the continuous phase and the jet orifice diameter is used as the dimensional length in Eq. (33). Equation (34) represents the body force to interfacial force balance within the emulsion and considers the relative density difference between the components. By dividing these two Bond numbers, a new nondimensional number, multiphase Bond number (Mu) results, a multiphase force balance between body forces and surface-to-interfacial tensions of the two liquids phases and gaseous phase in Eq. (35). These forces, balanced in the present form, are used to evaluate the contributions of the additional forces present in an emulsion. In Eq. (35), the dimensional lengths have also been split and reinterpreted in order to provide the appropriate length scale, with the trajectory height (y/d) used instead of (D_{32d}/d) to track the deviation due to body forces, while (D_{32d}/d) tracks the relative contribution of the cohesive surface tension versus breaking interfacial forces. Note, the absolute value of the density difference ($\rho_d - \rho_c$) is used in Eq. (35). The $\sigma_s D_{32d}/\sigma_i d$ term represents a force balance by a ratio of tension forces in respect to their physical length scale. Attributing the difference in body forces as the dominant factor influencing spray droplet size, based on the jet in crossflow trajectory results in Sec. 4.2, if component densities are equal, the plume trajectory will remain unaffected, resulting in Mu = 0.

$$\mathrm{Bo}_{l-g} = \frac{\rho_e g d_o^2}{\sigma_s}, \tag{31}$$

$$\mathrm{Bo}_e = \frac{(\rho_d - \rho_c) g D_{32d}^2}{\sigma_i} \tag{32}$$

$$\mathrm{Mu} = \frac{\mathrm{Bo}_e}{\mathrm{Bo}_{l-g}} = \frac{(\rho_d - \rho_c) y}{\rho_e d} \frac{\sigma_s D_{32d}}{\sigma_i d}. \tag{33}$$

If the discrete component density is larger than the continuous component within the jet, as it is in the current case with water, a difference in component momentum

will produce a larger concentration of the discrete phase liquid at higher trajectories. This has already been well documented by past experiments with injecting emulsions in pressure swirl nozzles (Bolszo, 2011; Bolszo et al., 2010; Narvaez et al., 2011). Also, injection as an emulsion results in measured droplet size distribution shifting to larger droplets at locations farthest from the injection wall but with little change near the wall. This signifies that the interfacial forces interact with the surface forces with increasing influence along the curved jet trajectory. It appears that DF2 is stripped off the column first, due to its lower surface tension versus water and higher concentrations of water remain in the core of the liquid jet column. The interfacial tension will then have greater influence in the jet breakup, creating ligaments which have higher momentum than the pure diesel fuel and are of larger size due to being composed of predominantly water (comparing Fig. 15 for water to Fig. 13 and Fig. 14). This effect will then produce larger droplet sizes at higher vertical trajectories.

To avoid a redundant y/d term [Eq. (31)] from being added to the established D_{32} relationship for pure liquids using the Buckingham π approach, a mathematical formulation introducing a S polynomial term for emulsions is sought in Eq. (36). Polynomial S will have n roots, Eq. (37), which is able to capture a higher order trend behavior. Results from tests have shown emulsions to both decrease and increase the spray's droplet size depending on emulsion composition and spray properties (Bolszo, 2011; Bolszo et al., 2010). If the water mass fraction is used as an indication of the emulsion discrete mass content, no contribution from the S term should occur at $\Phi = 0$ and $\Phi = 1$. Since the current study did not systematically vary the emulsion properties to achieve a full variation of an emulsion's influence on spray behavior, only a subset of roots will be utilized for the current work, posed mathematically as two roots, $\Phi = 0$ and $\Phi = 1$. Note that additional roots would include the $sole$ contribution of the surface-to-interfacial tension forces of the S term; which was eliminated due to not demonstrating a direct influence on improving breakup in the current work. Based on observed measurements, an increase in droplet size would occur with the introduction of a dispersed phase and a positive contribution would result. Therefore the equation form $S = 1 - \mathrm{Mu}\,\Phi(\Phi - 1)$ is proposed, where Mu would represent the contribution from the surface and body forces in Eq. (35). The resultant relationship is shown below in Eq. (38).

$$S = a_n\Phi^n + a_{n-1}\Phi^{n-1} + \ldots + a_2\Phi^2 + a_1\Phi + a_o, \tag{34}$$

$$(\Phi - A_n)(\Phi - A_{n-1})\ldots(\Phi - A_1)(\Phi - A_o), \tag{35}$$

$$S = 1 - \left(\frac{\rho_d - \rho_c}{\rho_e}\right)\left(\frac{\sigma_s D_{32d} y}{\sigma_i d^2}\right)(\Phi^2 - \Phi), [0 \leq \Phi < 0.5, 0.5 < \Phi \leq 1.0]. \tag{36}$$

Plugging the current fluid properties into Eq. (38) and selecting a representative dimensional length scale at a general height of y = 40 mm for the 0.57 mm diameter nozzle provides the relation for S in Fig. 19. D_{32d} values for stabilized emulsions vary from 1.5

to 10 μm and have been observed previously (Bolszo, 2011; Bolszo et al., 2010). For the current unstable emulsion cases and considering the shear forces produced by the static mixer, it is estimated that all cases will have D_{32d} values of 10–30 μm.

Physically, near a Φ value of 0.5, an inversion from a water-in-oil to an oil-in-water emulsion occurs, and a discontinuity results mathematically. Therefore, Eq. (36) must be applied as a piecewise function for $0 \leq \Phi < 0.5$ and at $0.5 < \Phi \leq 1$. The test conditions for the present work are overlaid on the S function in Fig. 19 at values on or very near Φ = 0, 0.23, 0.38, and 1.00. The S term is now added to Eq. (30) in Eq. (38) and the exponent G is determined.

$$\frac{D_{32}}{d} = 9.33 \times 10^7 \left(\frac{y}{d}\right)^{1.173} q^{-1.711} \mathrm{Re}_g^{-2.087} \mathrm{We}_{\mathrm{aero}}^{-0.419} S^G. \tag{37}$$

The contributions of the $\mathrm{Oh}_L$and the Re_L were also reevaluated in the current integration step for the entire data set (pure liquids and emulsions) and no additional improvement in fit was observed. S's exponent of G = 2.002 resulted from the linear regression analysis resulting in Eq. (38).

$$\frac{D_{32}}{d} = 9.33 \times 10^7 \left(\frac{y}{d}\right)^{1.173} q^{-1.711} \mathrm{Re}_g^{-2.087} \mathrm{We}_{\mathrm{aero}}^{-0.419} S^{2.002}. \tag{38}$$

The performance of Eq. (38) for emulsions is indicated in Fig. 20, which shows a high R^2 = 0.95421 and a linear fitted slope of 1.01537. Evaluating the linear fit of Eq. (38) for all the cases, pure DF2, water, and emulsion cases, a goodness-of-fit

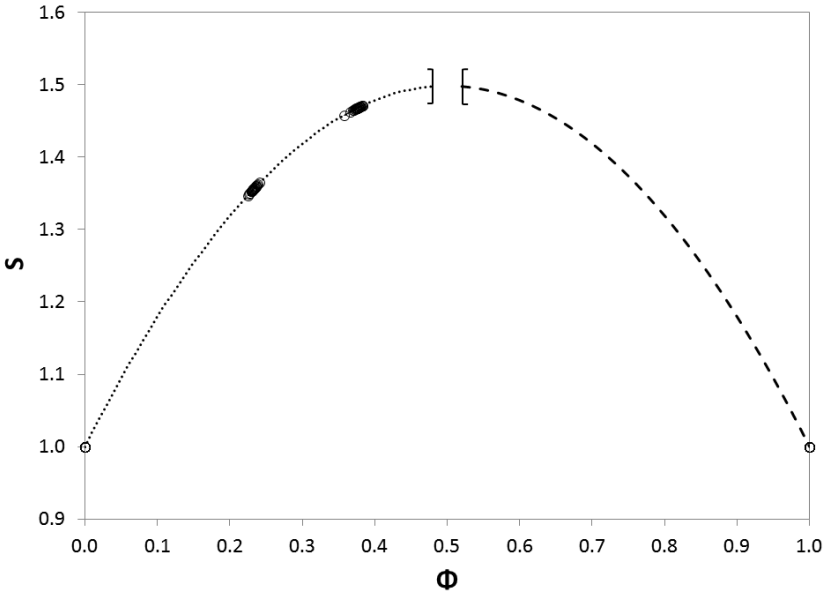

FIG. 19: Tension-to-body force parameter (S) variation with water droplet fraction.

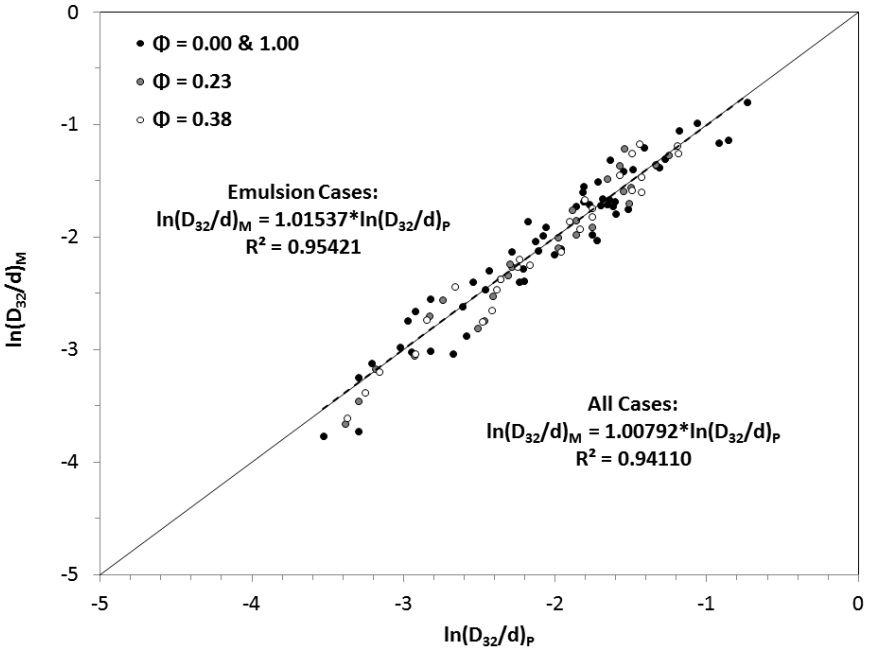

FIG. 20: Linearized measured jet in crossflow droplet size versus correlated droplet size for pure fuels using Eq. (38) and corresponding goodness-of-fit parameters.

R^2 = 0.94110, with a linear fitted slope of 1.00792. The fit of the complete data set is demonstrated in Fig. 21 with the correlation trend line overlaid.

The resultant plume droplet size correlation [Eq. (38)] is now applied to the current data to test the fit for the pure components in Fig. 22 and Fig. 23 and for the emulsion cases in Fig. 24. The overall fit is quite good for the small and medium size droplets considered. The effect of an emulsion on measured droplet sizes captures the modification toward larger sizes for the current experiments when comparing Fig. 18 and Fig. 21. The remaining spread in the measured values is present due mainly to the moderate amount of data which was used to derive the current equation. Note that this evaluation occurred at a single downstream x value of 40 mm. Also, considerations to use a representative jet length parameter along its center were not incorporated in order to provide a single vertical value at the jet height y at a given x.

4.5 Phenomenological Model for Emulsion Jet Breakup

Significant differences in jet breakup are observed between the liquid jet and emulsion jet for the same experimental test conditions. Specifically, the introduction of a discrete droplet distribution within the continuous liquid gives rise to an additional force influ-

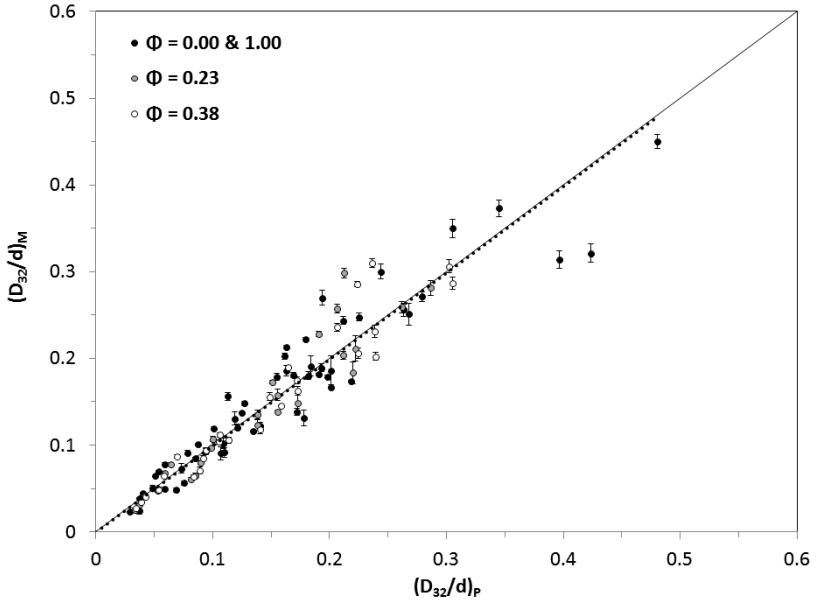

FIG. 21: Droplet size correlation [Eq. (38)] plotted for complete pure and emulsion droplet size dataset.

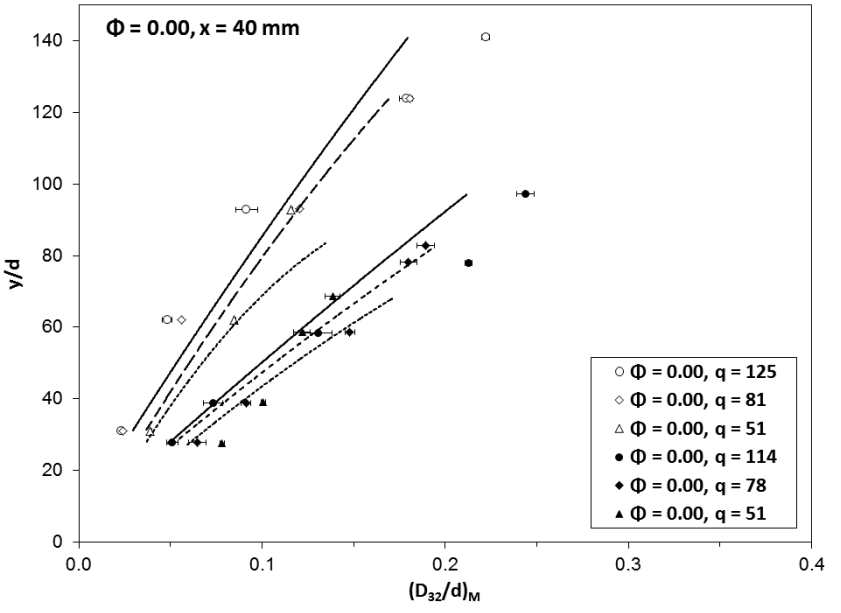

FIG. 22: Jet in crossflow droplet size measurements for pure oil with correlation [Eq. (38)] overlaid.

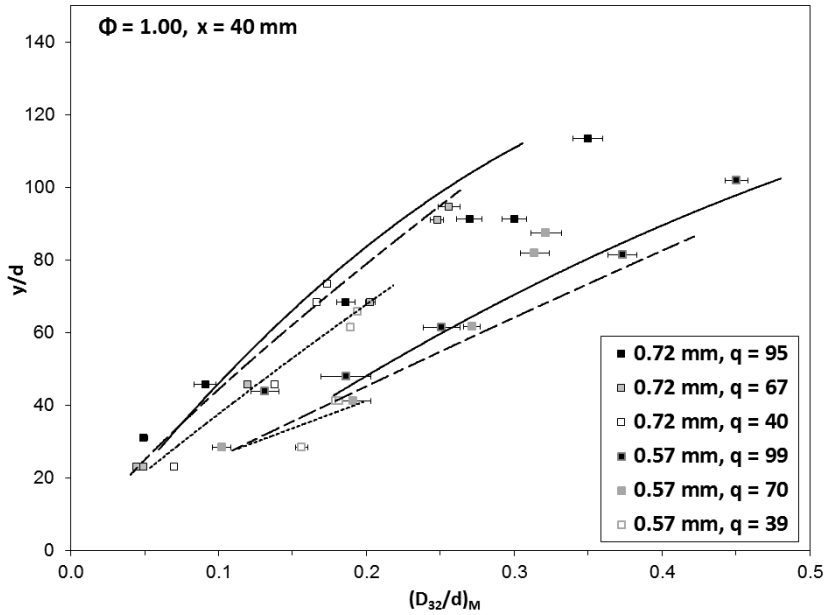

FIG. 23: Jet in crossflow droplet size measurements for pure water with correlation [Eq. (38)] overlaid.

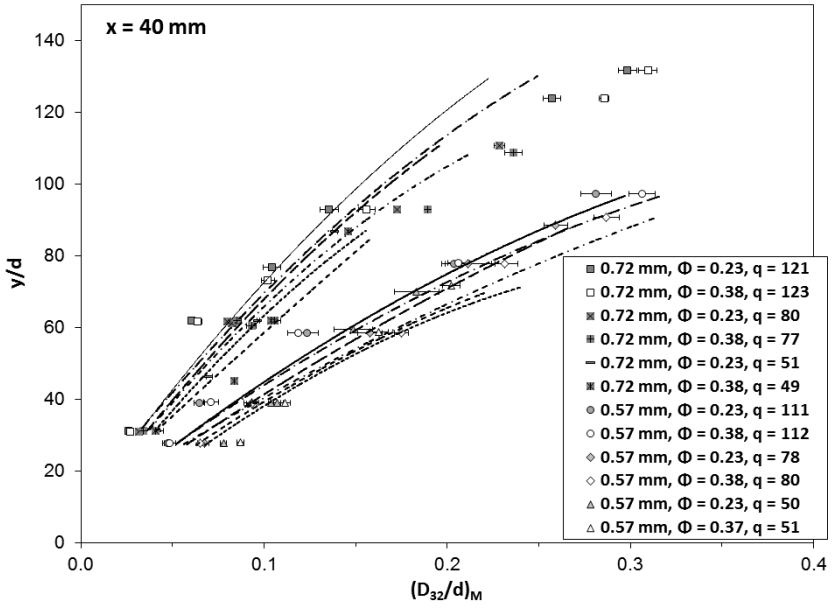

FIG. 24: Jet in crossflow droplet size measurements for water-in-oil with correlation [Eq. (38)] overlaid.

encing liquid breakup, the contribution from the interfacial force between the liquids. Referring to Fig. 25, this interfacial force is presented as a new primary breakup mode, in addition to the surface breakup and column breakup modes in Fig. 1(a). In Fig. 25, an emulsion jet in crossflow diagram is presented at low We_{aero}. Differences in breakup can be recognized by comparing Fig. 25 with Fig. 1 schematically to actual high-speed snapshots in Fig. 26. Evidence of the interfacial breakup mode during the evolution of the emulsion jet in crossflow is initially observed by minute perforations in the liquid column, in the near field of the nozzle exit. These perforations grow rapidly in the current experiment, penetrating into the column's core, creating a gas-filled void and leading to an earlier pinch-off of the jet compared to the pure jets of both components. In Fig. 26, the result of these minute perforations is shown to be the earlier pinch-off point in the emulsion case versus DF2, as well as multiple pinched-off segments prior to the formation of traditional long ligaments. The initial location where perforations occur appears to have no preference along the column cross section (e.g., windward or leeside), suggesting that the variation and position of the internal distribution of discrete droplets within the column may give rise to perforations forming. These voids increase

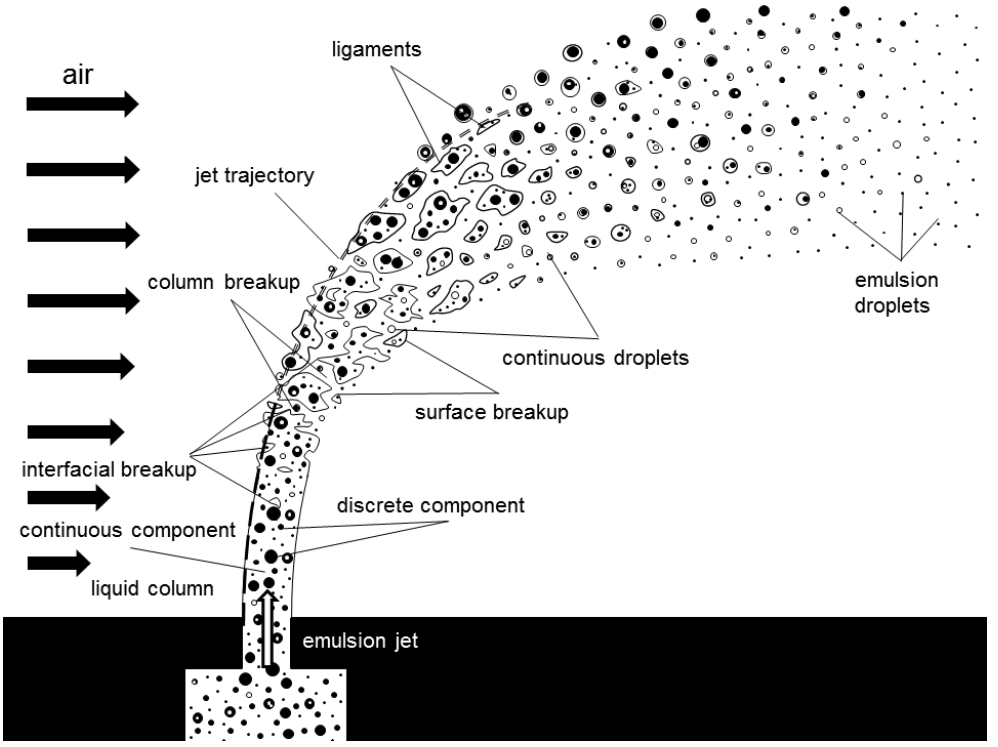

FIG. 25: Representative schematic of primary breakup in an emulsion jet in crossflow at low We_{aero}.

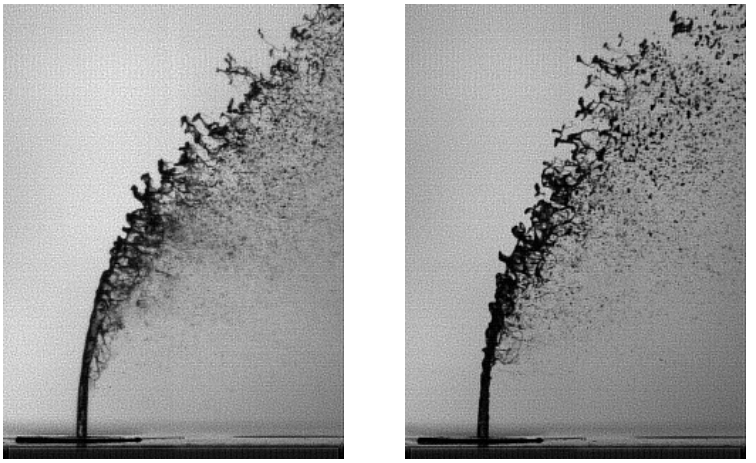

d = 0.72 mm, Φ = 0.00, q = 118 d = 0.72 mm, Φ = 0.38, q = 120

FIG. 26: Snapshots of DF2 and an emulsion jet in crossflow at We_{aero} = 48 (low cases).

the surface area for air to interact with the column and better transferring momentum between the three fluids. Also, these ligaments break up more quickly due to the interfacial forces, in turn producing shorter initial ligaments after pinch-off. The influence of interfacial forces for discrete droplet laden (dilute emulsions) liquid sheets in a quiescent environment has been well documented by Dombrowski and Fraser (1954).

The overall pinch-off distance of the column occurs earlier for the emulsion jet column versus the pure jet column for the experiment. This appears again to be due to the influence of the interfacial breakup as a contributing force. The result of the earlier pinch-off is a more widely dispersed plume of droplet trajectories in the vertical (y) direction, shown when comparing Fig. 25 and Fig. 1. The presence of discrete droplets within the jet appears to stiffen the column in terms of dampening Kevin–Helmholtz instabilities. Together, these two processes lead to a smaller contribution from the column breakup mode and the additional interfacial breakup force contributes to an equal order of magnitude. The result is observed as fractures due to instability versus pinching off from the column much earlier in the evolution of the plume.

The leading edge of the crossflow provides another distinctive breakup phenomenon for emulsions. Considering water as the discrete component within DF2 oil, which has a higher density (Table 1), will equate to a larger overall penetration trajectory for the emulsion versus a DF2 column alone with Eqs. (5) and (26). However, the resultant spray droplets demonstrate a stratification of droplet size with increased y distance. At the current conditions, laser diffraction measured emulsion jet droplets were larger in size, the same size as well as smaller in size compared to pure DF2 oil jets along the same corresponding regions of the plume (Bolszo, 2011). At the top edge of the spray, the largest droplets were found to exist, significantly larger than those of DF2's top

edge, suggesting, based on the present set of penetration results, that water is present in higher concentrations at higher trajectories. The largest droplets have been observed to penetrate much farther in to the crossflow, which are generated less frequently the larger they become, existing as rogue droplets, as shown schematically in Fig. 25 and Fig. 27, as well as observed visually in comparing both cases in Fig. 28.

Important similarities between the pure liquid and emulsion jets have been quantified as well. In the jet near field, the first droplets to be stripped off the emulsion column are the same size as those of the pure DF2. An emulsion jet in crossflow at high We_{aero} in Fig. 27 is compared with the pure liquid case in Fig. 2 to compare the breakup process. Perforations in the jet exist in Fig. 27 and Fig. 28, as in Fig. 25 and Fig. 26. However, due to the intensified surface breakup at these corresponding conditions, the overall jet breakup presents less overall structure and a quicker and more compact transition to a spray plume. The largest droplets, illustrated to be composed of primarily water, are shown to penetrate further into the crossflow versus the bulk of the emulsion with the continuous oil component. The location and droplet size of the stripped droplets are based on observation and laser diffraction measurements made downstream, reported elsewhere (Bolszo, 2011). The matching droplet size measured in the near-wall region for the emulsion and pure DF2 cases is due to the lower surface tension of the oil compared to the dispersed water droplets in the emulsion, allowing DF2 to be stripped off

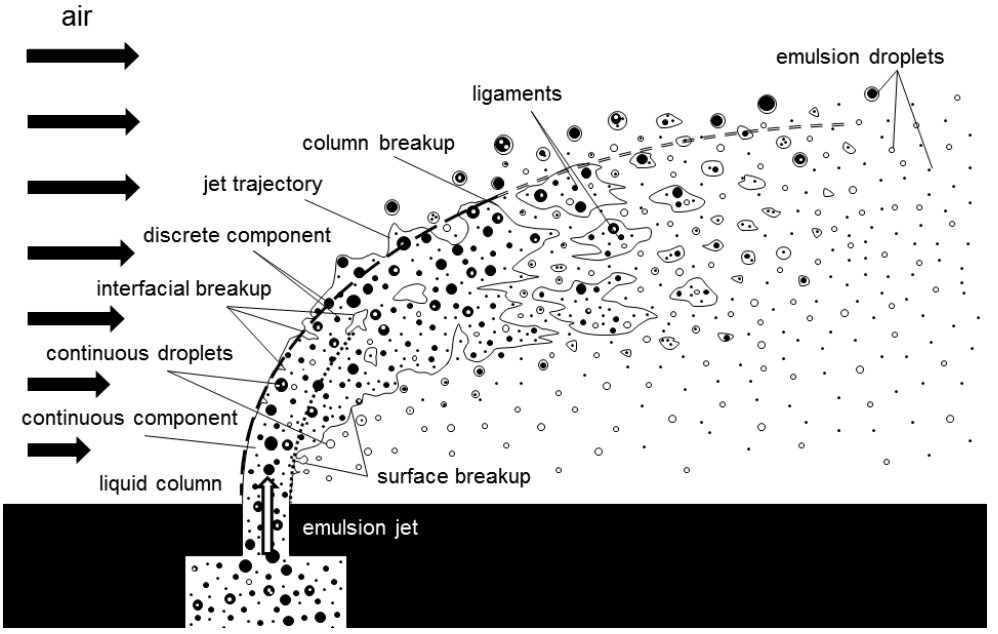

FIG. 27: Representative schematic of primary breakup in an emulsion jet in crossflow at high We_{aero}.

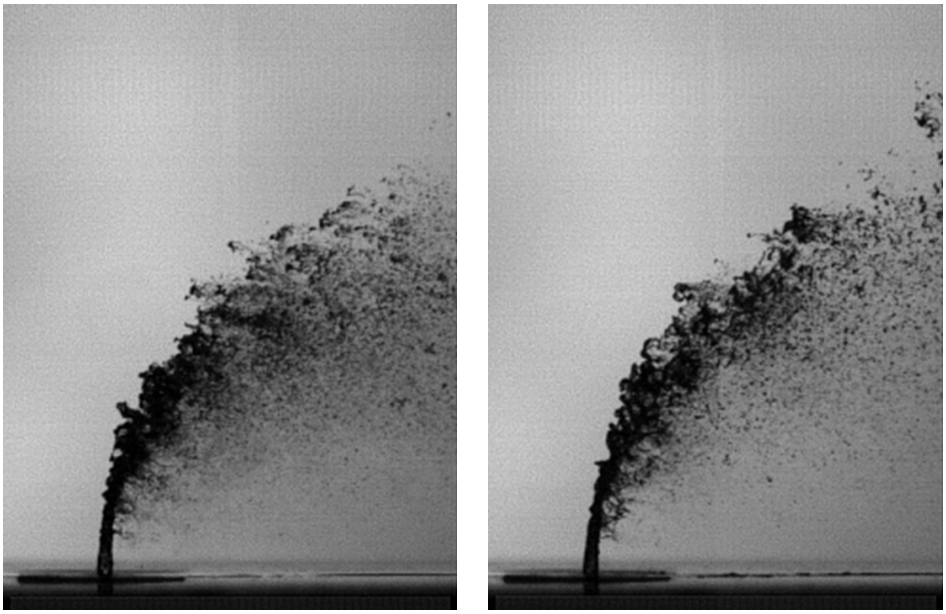

d = 0.72 mm, Φ = 0.00, q = 49 d = 0.72 mm, Φ = 0.39, q = 48

FIG. 28: Snapshots of DF2 and an emulsion jet in crossflow at We_{aero} = 120 (high cases).

more easily, resulting in an absence of water in this region. Specifically, this implies that no or very little actual water droplets are sheared off the surface; however, small water droplets stripped off with the sheared continuous oil component can end up within the resultant emulsion droplet formed.

5. SUMMARY AND CONCLUSIONS

The penetration of liquid jets and the resultant plume droplet size of natural unstable emulsions into a crossflow was investigated and reported, to the best of the authors' knowledge, for the first time. Experiments were carried out at atmospheric conditions for pure diesel fuel, two emulsion concentrations, and three crossflow air flow rates. Two nozzle diameters were investigated. The Buckingham π theorem was used to identify the governing fluid processes through fluid parameters which are responsible for breaking up of an emulsion liquid jet in the current geometry for the first time. Results show that the penetration of emulsions can be predicted by simple versions of well-established equation form by Geery and Margetts (1969) and correlation values of Wu and co-workers (1998). As a result, the trajectory of emulsions is predominantly dictated by the momentum flux ratio considering an emulsion density of the bulk fluid, without the significant influence of interfacial forces. Deviations in fit were attributed to differ-

ences in the dominant breakup mechanisms between the nozzles and are elucidated by observation as well as justified by governing physics from a dimensional analysis. This approach was first performed to arrive at the current jet in crossflow equation forms previous reported in the technical literature. Even with the more complex emulsion jets, a simple correlation provides an excellent fit with a simple two term correlation [Eq. (27)] for both emulsion and pure fuel cases.

$$\frac{y}{d} = 1.48\left(q\frac{x}{d}\right)^{0.43}. \tag{27'}$$

This approach was then applied in order to determine the physical processes responsible for determining the resultant jet and emulsion jet in crossflow droplet size distribution within the plume cross section. The current grouping presents a new set of nondimensional numbers which is different from past studies (Kihm et al., 1995) and is favorable for its use of the momentum flux ratio q and simple form. A new multiphase nondimensional number was defined, the multiphase Bond number (Mu = $\mathrm{Bo}_e/\mathrm{Bo}_{l-g}$), to balance the body-to-surface force balance for the current three-fluid component problem in order to quantitatively capture the influence the discrete emulsion droplets have on breakup. A new term (S) was introduced that evaluates the magnitude of the interfacial-to-surfaces forces as well as the role of discrete-to-continuous component momentum contributions [Eq. (38)]. The current correlation utilizes a simplified two root polynomial form, $\Phi = 0$, $\Phi = 1$ selected based on measured test conditions.

$$S = 1 - \left(\frac{\rho_d - \rho_c}{\rho_e}\right)\left(\frac{\sigma_s D_{32d} y}{\sigma_i d^2}\right)(\Phi^2 - \Phi), [0 \le \Phi < 0.5, \Phi = 1] \tag{36'}$$

$$\frac{D_{32}}{d} = 9.33 \times 10^7 \left(\frac{y}{d}\right)^{1.173} q^{-1.711}\mathrm{Re}_g^{-2.087}\mathrm{We}_{\mathrm{aero}}^{-0.419} S^{2.002}. \tag{38'}$$

This S term was included to account for the effects of an emulsion on increasing jet in crossflow droplet size in Eq. (38). The resultant correlation, also determined through a linear regression analysis, provided a good predictive fit with the current pure component and emulsion laser diffraction droplet size data. Additional tests are needed in order to broaden the correlation's application to varying x positions, varying emulsion compositions (D_{32d}, Φ) and to determine the effect of the liquid (nozzle) Reynolds number Re_N.

ACKNOWLEDGMENTS

Siemens Power Generation partially supported this work under the Oil Emulsions Project. A special thanks to our laboratory Research Engineer, Richard Hack, for his aid and support in facilitating regular laboratory operations and ensuring a safe experimental environment.

REFERENCES

Adelberg, M., Breakup rate and penetration of a liquid jet in a gas stream, *AIAA J.*, vol. **5**, no. 8, pp. 1408–1415, 1967.

Becker, J. and Hassa, C., Breakup and atomization of a kerosene jet in crossflow at elevated pressure, *Atomization Sprays*, vol. **12**, pp. 49–68, 2002.

Birouk, M., Iyogun, C. O., and Popplewell, N., Role of viscosity of trajectory of liquid jets in a cross-airflow, *Atomization Sprays*, vol. **17**, pp. 267–287, 2007.

Bolszo, C. D., *Pressure atomization of water-in-oil emulsions and the effect of gaseous crossflow*, PhD Dissertation, University of California, Irvine, 2011.

Bolszo, C. D., Narvaez, A. A., McDonell, V. G., Dunn-Rankin, D., and Sirignano, W. A., Pressure-swirl atomization of water-in-oil emulsions, *Atomization Sprays*, vol. **20**, no. 12, pp. 1077–1099, 2010.

Brown, C. T. and McDonell, V. G., Near field behavior of a liquid jet in a crossflow, in *ILASS Americas 19th Annual Conf. on Liquid Atomization and Spray Systems*, Toronto, Canada, May 23-26, 2006.

Brown, C. T., Mondragon, U. M., and McDonell, V. G., Effect of nozzle discharge coefficient on penetration of a plain liquid jet injected into a crossflow, Presented at *ILASS-Americas 2007*, Chicago, IL, May 15-18, 2007.

Clark, B. J., Breakup of a liquid jet in a transverse flow of gas, NASA TN D-2424, 1964.

Dombrowski, N. and Fraser, R. P., A photographic investigation into the disintegration of liquid sheets, *Trans. R. Soc. London, Ser. A., Math. Phys. Sci.*, vol. **247**, no. 924, pp. 101–130, 1954.

Geery, E. L. and Margetts, M. J., Penetration of a high velocity gas stream by a water jet, *J. Spacecr.*, vol. **6**, no. 1, pp. 79–81, 1969.

Gonzalez, R. C., Woods, R. E., and Eddins, S. L., *Digital Image Processing Using Matlab*, Pearson Prentice Hall, Upper Saddle River, NJ, p. 405, 2004.

Herrmann, M., Detailed numerical simulations of the primary atomization of a turbulent liquid jet in crossflow, *J. Eng. Gas Turbines Power*, vol. **132**, pp. 061506-1–10, June, 2010.

Hinze, J. O., Fundamentals of hydrodynamic mechanisms of splitting in dispersion processes, *AIChE J.*, vol. **1**, no. 3, pp. 289–295, 1955.

Jalaal, M. and Mehravaran, K., Fragmentation of falling liquid droplets in bag breakup mode, *Int. J. Multiphase Flow*, vol. **47**, pp. 115–132, 2012.

Kihm, K. D., Lyn, G. M., and Sun, S. Y., Atomization of cross-injecting sprays into convective air stream, *Atomization Sprays*, vol. **5**, pp. 417–433, 1995.

Krieger, I. M. and Dougherty, T. J., A mechanism for non-Newtonian flow in suspensions of rigid spheres, *Trans. Soc. Rheol.*, vol. **3**, pp. 137–152, 1959.

Krynke, K. K. and Sek, J. P., Predicting viscosity of emulsion in the broad range of inner phase concentrations, *Colloids Surf. A: Physicochem. Eng. Aspects*, vol. **245**, pp. 81–92, 2004.

Krzeczkowski, S. A., Measurement of liquid droplet disintegration mechanisms, *Int. J. Multiphase Flow*, vol. **6**, no. 3, pp. 227–239, 1980.

Lee, K., Aalburg, C., Diez, F. J., Faeth, G. M., and Sallam, K. A., Primary breakup of turbulent round liquid jets of uniform crossflows, *AIAA J.*, vol. **45**, no. 8, pp. 1907–1916, 2007.

Leong, M. Y, *Mixing of an Airblast-Atomized Fuel Spray Injected into a Crossflow of Air*, PhD Thesis, University of California, Irvine, 2000.

Leong, M. Y, McDonell, V. G., and Samuelsen, G. S., Effect of ambient pressure on an airblast spray injected into a crossflow, *J. Propuls. Power*, Sept.-Oct., vol. **17**, no. 5, pp. 1076–1084, 2001.

Lubarsky, E., Reichel, J. R., Zinn, B. T., and McAmis, R., Spray in crossflow: Dependence on Weber number, *J. Eng. Gas Turbines Power*, vol. **132**, pp. 021501-1–9, Feb., 2010.

Narvaez, A. A., Bolszo, C. D., McDonell, V. G., Dunn-Rankin, D., and Sirignano, W. A., Comparison of oil-in-water characteristics for low and high capacity pressure-swirl nozzles, *Atomization Sprays*, vol. **12**, pp. 391–410, 2011.

Otsu, N., A threshold selection method from gray-level histograms, *IEEE Trans. Systems, Man, Cybern.*, vol. SMC-**9**, no. 1, pp. 62–66, 1979.

Ouchiyama, N. and Tanaka, T., Estimation of the average number of contacts between randomly mixed solid particles, *Ind. Eng. Chem. Fundam.*, vol. **19**, pp. 338–340, 1980.

Pal, R., A novel method to correlate emulsion viscosity data, *Colloids Surf. A: Physicochem. Eng. Aspects*, vol. **137**, pp. 275–286, 1998.

Rachner, M., Becker, J., Hassa, C., and Doerr, T., Modeling of the atomization of a plain liquid fuel jet in crossflow at gas turbine conditions, *Aerospace Sci. Technol.*, vol. **6**, pp. 495–506, 2002.

Sallan, K. A., Aallberg, C., and Faeth, G. M., Breakup of round nonturbulent jets in a gaseous crossflow, *AIAA J.*, vol. **42**, no. 12, pp. 2529–2540, 2004.

Schetz, J. A. and Padhye, A., Penetration and breakup of liquids in subsonic airstreams, *AIAA J.*, vol. **15**, no. 10, pp. 1385–1390, 1977.

Stenzler, J. N., Lee, J. G, and Santavicca, D. A., Penetration of liquid jets in a crossflow, in *AIAA, Aerospace Sciences Meeting & Exhibit*, Reno, NV, Paper 2003–1327, Jan. 6-9, 2003.

Wu, P., Kirkendall, K. A., Fuller, R. P., and Nejad, A. S., Breakup process of liquid jets in subsonic crossflows, *J. Propuls. Power*, vol. **13**, no. 1, pp. 64–73, 1998.

Wu, P., Kirkendall, K. A., Fuller, R. P., and Nejad, A. S., Spray structure of liquid jets atomized in subsonic crossflows, *J. Propuls. Power*, vol. **14**, no. 2, pp. 173–182, 1998.

APPENDIX A: DIMENSIONAL ANALYSIS

A dimensional analysis was performed to predict the functional dependence on fluid properties on emulsion jets in crossflow penetration, vertical position y in the spray near field, and resultant downstream droplet size within the spray plume (spray Sauter mean diameter, D_{32}). As an example, a generalized relation is provided to demonstrate the current treatment in Eq. (A1). The Buckingham π theorem is used to nondimensionalize the functions in groupings [Eq. (A2)]. Elimination of certain nondimensional groupings was performed for parameters which were not varied extensively. In order to evaluate these consequent nonlinear multiplicative functions using the least-squares method for the experimental data provided, the natural log function was applied to both sides of the

equation to linearize the contribution from their exponents as well as the multiplicative constant, as treated from Eq. (A3) to (A4). The results are processed and the linear fit is optimized using a statistical solver. The exponential function is then applied to both sides of the equation to return the resultant equation to its original, single term form with its exponents and prefactor constant now determined. These resultant relations are what are plotted on the correlation plots, however the R^2 values are taken from the fit of the linearized equations.

$$G \sim f(B, C, E, ..., I, J), \tag{A1}$$

$$\Pi_1 \sim f(\Pi_2, \Pi_3, \Pi_4, ..., \Pi_n), \tag{A2}$$

$$\Pi_1 = a\,(\Pi_2)^b\,(\Pi_3)^c\,(\Pi_4)^e \ldots (\Pi_n)^r\,, \tag{A3}$$

$$\ln(\Pi_1) = A + b\ln(\Pi_2) + c\ln(\Pi_3) + e\ln(\Pi_4) \ldots r\ln(\Pi_n)\,. \tag{A4}$$